Acta Cryst. (1962). **15**, 983

Single-Crystal Intensity Measurements with the Three-Circle Counter Diffractometer

BY LEROY E. ALEXANDER AND GORDON S. SMITH

Mellon Institute, Pittsburgh 13, *Pennsylvania, U.S.A.*

(*Received* 26 *June* 1961 *and in revised form* 27 *December* 1961)

An analysis is given of some important experimental factors governing the generation of reflections from single crystals and their measurement by means of counters. When no monochromatization is employed other than that provided by β filters, the moving crystal-moving counter (2θ-scan) technique is in principle best suited to reliable measurements of integrated reflection intensities, $I_i(hkl)$. Under certain experimental conditions the Cauchy-like shape of the spectral component of the intensity profile necessitates corrections for losses resulting from the finite range of scan. Because of spectral dispersion I_i cannot be accepted as proportional to I_p, the peak intensity, except in a limited low-θ region. However, it is possible to establish correction curves to convert measured I_p's to I_i's with reasonable accuracy. Recommendations are given for optimizing the conditions of measurement including algebraic expressions for the acceptable values of the crystal mosaicity and sizes of the crystal, X-ray source, and receiver aperture as imposed by the geometrical constraints of the apparatus.

1. Introduction

The past twelve years have witnessed a rapid development in the use of counter diffractometers for the measurement of single crystal intensities. Exploratory studies by Lonsdale (1948) and by Wooster, Ramachandran & Lang (1948) were followed by a more extensive investigation by Cochran (1950), who showed that counter techniques are inherently capable of considerably higher precision than photographic methods. Soon thereafter efforts were made to adapt Weissenberg cameras to Geiger-counter measurements (for example, Clifton, Filler & McLachlan, 1951; Evans, 1953), but with somewhat mixed success. Renewed impetus to developments in counter apparatus was provided by the introduction of proportional and scintillation counters and by the invention of the 'Eulerian cradle' goniostat by Furnas & Harker (1955) which facilitated intensity measurements by (1) utilizing the more convenient geometry of the 'flat-cone' technique (Buerger, 1942) and (2) extending the range of data accessible with a single mounting of the crystal. In a subsequent modification of this instrument further advantages were gained by changing the χ range from $(-53°-+53°)$ to $(-10°-+100°)$ (Furnas, 1957).

As early as 1955 and especially very recently attention has tended to focus on the problem of reducing the labor of gathering counter intensity data by means of automatic control systems (Bond, 1955; Benedict, 1955; Drenck, Diamant & Pepinsky, 1959; Ladell & Lowitzsch, 1960; Brown & Forsyth, 1960; Arndt, 1960; Ladell, Spielberg & Lowitzsch, 1960; Clastre, 1960; Arndt & Phillips, 1961). In toto the current investigations represent a very costly and impressive investment in personnel time and instrumentation, which is, of course, some indication of the great importance which crystallographers attach to the problem of removing this major barrier in the path of effective solution of complex crystal structures.

The authors feel that perhaps already overdue is a careful appraisal of the more basic systematic factors which must be reckoned with in the process of measuring integrated intensities with counters. The ensuing treatment encompasses the following principal topics: (1) analysis of the 2θ- and ω-scan techniques on the basis of the reciprocal lattice concept, (2) synthesis of reflection profiles by the convolution method, (3) development of correction curves for the effect of limited scanning ranges, (4) derivation of curves for the conversion of peak to integrated intensities, (5) discussion of the accuracy in lattice constants required for the determination of the crystal orientation settings, (6) practical recommendations. Item (4) constitutes a critical evaluation of the contention frequently voiced that under appropriate conditions the intensity diffracted by a stationary crystal is proportional to the integrated intensity (Cochran, 1950; Lang, 1954; Furnas & Harker, 1955; Furnas, 1957). The significant findings of the present investigation may be grasped by reading only the main text; the more determined reader will find in the appendixes a detailed exposition of some of the underlying geometrical X-ray optics. In particular we may note the presence of material relative to the concept of integrated intensity in Appendixes A and B and to the choice of receiving aperture dimensions in Appendix D.

The ultimate goal of this study was to develop procedures for measuring relative intensities with high reliability without paying an undue penalty in time expended. In pursuing this goal we have examined the sources of deviations of the experimental inten-

sities from their ideal values, and this has served to supply a basis for criteria of acceptability. Although the end sought has necessitated a degree of compromise between accuracy and speed, chief emphasis has been placed on accuracy. In behalf of speed and simplicity of technique, however, in the present paper we consider only the case of an incident beam taken directly off the focal spot of the X-ray tube with no monochromatization other than that provided by β filters and the natural response curve of the counter.

In the interests of economizing space little or no mention will be made of errors due to crystal misalignment, counting statistics, extinction, absorption of X-rays by the crystal, and time-wise variation in direct beam intensity. It will be assumed that care has been exercised to minimize errors of these kinds. In the present study the experimental data were measured with a General Electric XRD-5 diffraction unit equipped with a Single Crystal Orienter (Furnas, 1957) and a krypton-filled proportional counter. The collimators were modified as required by the investigation.

2. General experimental conditions

We adopt the conventions employed by Furnas (1957) and later recommended for standardization by Arndt & Phillips (1958) in designating the three crystal orientation axes as shown in Fig. 1: ω (also θ and 2θ),

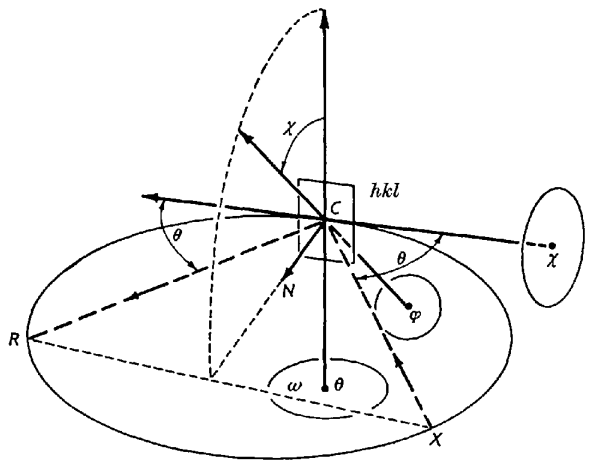

Fig. 1. Geometry of the three-circle single-crystal diffractometer.

rotation about the vertical axis of the diffractometer; χ, angle of inclination about a horizontal axis; and φ, rotation about the axis of the goniometer head (or azimuth). X is the center of the focal spot, C the center of the crystal, and CR the direction of the beam diffracted by the planes (hkl). CN is the plane normal. It will be assumed that intensities are to be recorded by the 'flat-cone' technique (Buerger, 1942), which necessitates that the reflections be brought into the equatorial plane, XCR, by appropriately tilting the crystal using the χ motion.

Some additional experimental conditions remain to be specified: (1) The focal spot is viewed at such an angle that its projection is at least approximately equidimensional. (2) The crystal dimensions are much smaller than the dimensions of the projected focal spot. (3) The direct beam is not collimated in the usual sense; it is surrounded over much of its length by an 'anti-scatter' cylindrical tunnel of an aperture sufficient to permit all points on the crystal to 'view' all points on the focal spot without obstruction. (4) Likewise the diffracted beam collimator is cylindrical and of sufficient aperture to cause no obstruction of the diffracted beam, which means that its only function is to exclude unwanted radiation from the counter. (5) It is assumed that the portion of the counter window exposed by the receiving aperture is uniformly sensitive to the diffracted X-rays.

In Appendixes A and B it is shown that when a crystal of negligible absorption for the X-ray beam of wavelength λ_0 is turned through the entire angular range corresponding to diffraction from any given planes (hkl), every point on the crystal diffracts X-rays originating at every point on the source. Under these circumstances and those prescribed in the preceding paragraph, every volume element of the crystal contributes with equal weight to the over-all diffracted energy.* This over-all energy we shall regard in the present paper as a measure of the *integrated reflection intensity*, $I_i(hkl)$. It is implicit in this definition that in any actual measurement an appropriate correction will be made for diffracted energy due to wavelengths other than λ_0. In an actual experiment it is evident that a discrete wavelength, λ_0, cannot be attained, for which reason we shall regard λ_0 as referring to the particular narrow distribution of wavelengths comprising a given spectral line, for example, $K\beta, K\alpha_1, K\alpha_2$, or the combined doublet $K\alpha_{1,2}$. In regard to the concept of integrated intensity the reader is also referred to Compton & Allison, 1935, pp. 405–15, and Furnas, 1957, pp. 71 and 99.

3. Conditions of measurement: Idealized case

We wish to consider first the idealized case of diffraction involving (1) a perfect point crystal, (2) a point source of truly monochromatic X-rays, and (3) a receiving aperture of non-critical size. However, in order to preserve the validity of certain quantitative arguments in the ensuing discussion, we shall find it necessary to replace items (1) and (2) by the very close approximations of (1) a very small, perfect crystal and (2) a very small source of truly monochromatic X-rays.

With reference to Fig. 2, the crystal is turned about the axis Q through an angle ω_0 chosen so that

* It is perhaps self-evident that this is also contingent upon the crystal's turning with uniform angular velocity.

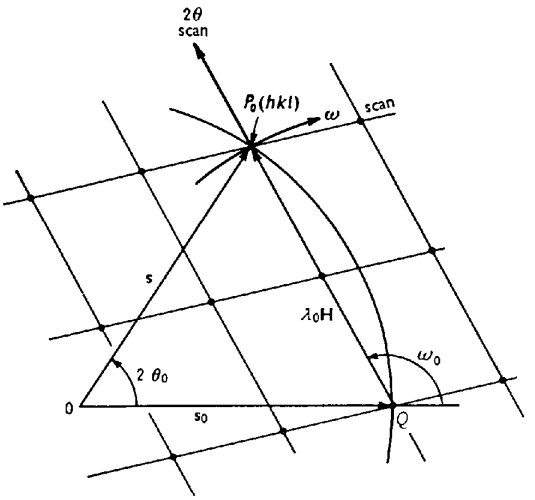

Fig. 2. Idealized reciprocal-lattice diagram of diffraction by planes (*hkl*) and measurement by the ω-scan and 2θ-scan techniques.

the desired reciprocal lattice point $P_0(hkl)$ on the equatorial net intersects the sphere of reflection. QP_0 is then the direction of the central lattice row line of which $P_0(hkl)$ is a member. The direct and diffracted beam vectors are, as customary, $\mathbf{s}_0$ and $\mathbf{s}$, the reciprocal lattice vector of the diffracting point $P_0(hkl)$ is $\lambda_0\mathbf{H}$, and the radius of the reflecting sphere is unity. We consider three simple experimental arrangements, all based on the flat-cone geometry (Furnas, 1957, Chapter VII):

1. Stationary crystal—stationary counter.
2. Moving crystal—stationary counter (ω scan).
3. Moving crystal—moving counter (2θ scan).

When the crystal is rotated to the position ω_0 and the receiver set at the angle $2\theta_0$, a very narrow diffracted ray enters the receiver. With stationary crystal and counter a measure of I_p, the peak intensity, can be obtained by recording the number of counts, N_t, received in a fixed period of time t. Next we leave the receiver set at the angle $2\theta_0$, mis-set the angular position of the crystal to $\omega_0-\delta\omega$, and then cause the crystal to turn at constant angular velocity from $\omega_0-\delta\omega$ to $\omega_0+\delta\omega$. As it passes through the reflecting angle ω_0, the point $P_0(hkl)$ intersects the sphere of reflection (following the circular path marked 'ω scan' in Fig. 2) and a number of counts is obtained which is a measure of I_i, the integrated intensity. Finally, if the motions of crystal and receiver are coordinated so that the angular velocity of revolution of the receiver is double that of rotation of the crystal ($2\dot{\omega}$ and $\dot{\omega}$ respectively), the receiver scans reciprocal space along the direction of a central lattice row line marked '2θ scan' and through the point $P_0(hkl)$, and once again some number of counts is obtained which is a measure of I_i.

In the above procedures we may observe that the reflected ray is very narrow, so that its intensity profile as a function of $\Delta\omega$ or $\Delta 2\theta$ is very sharp. In the ideal limiting case it becomes line-like (a delta function).

4. Conditions of measurement: Real case

We next consider the conditions prevailing when the X-ray beam is not strictly monochromatic (there is a wavelength dispersion of $\Delta\lambda/\lambda$), the crystal possesses finite dimensions and mosaic character, and the X-ray source has finite dimensions. These four factors have the effect of smearing out the discrete crystal orientation angle, ω_0, corresponding to the generation of a reflection (*hkl*) (contrast Fig. 3 with Fig. 2). Designating the above four factors by the respective subscripts λ, c, m, and x, we may describe each effect

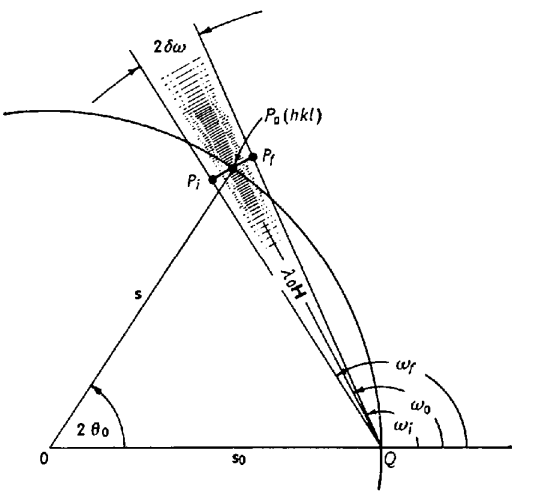

Fig. 3. Reciprocal-lattice diagram of diffraction by planes (*hkl*): Real case.

as an angular increment: $\pm\delta\omega_\lambda$, $\pm\delta\omega_c$, $\pm\delta\omega_m$, and $\pm\delta\omega_x$. These combine to produce an over-all angular range of orientation (Furnas, 1957, pp. 91 and 99),

$$2\delta\omega=2(\delta\omega_\lambda+\delta\omega_c+\delta\omega_m+\delta\omega_x)\,,$$

in which detectable intensity from the planes (*hkl*) is recorded by the counter located at the calculated angle $2\theta_0$. With reference to Fig. 3, detectable intensity will be recorded from the time P_i intersects the sphere of reflection until P_f does so. Wavelengths other than λ_0 diffracted by the reciprocal lattice point (*hkl*) produce a range in the length of the vector $\lambda\mathbf{H}$, which is indicated by the shaded zone of the figure. The amount of intensity due to these unwanted wavelengths which is received simultaneously when the receiver is set at the angle $2\theta_0$ depends upon the angular width, $\Delta 2\theta$, of the receiving aperture. On the other hand, when the crystal and receiver are both moved with the relative angular velocities $\dot{\omega}$ and $2\dot{\omega}$, the receiver searches in the direction of the central

lattice row line and therefore measures this entire band of wavelengths progressively.

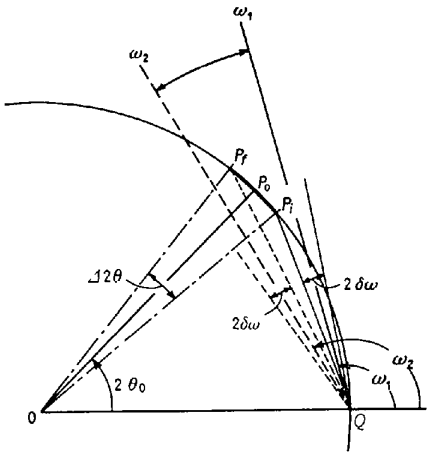

Fig. 4. Geometry of the ω scan.

Fig. 4 illustrates the ω-scan geometry. Because of the angular range of the receiving aperture, $\Delta 2\theta$, diffracted intensity is recorded from diffraction vectors, $\lambda\mathbf{H}$, terminating anywhere on the circle of reflection between points P_i and P_f (black segment of circle). Therefore, assuming an angular range of orientation of the crystal, $\pm\delta\omega$, as explained above, with the receiver centered at the angle $2\theta_0$, finite diffracted intensity will be recorded for all orientations of the crystal in the range ω_1 to ω_2. Furthermore this involves contributions from a range of wavelengths extending from $|\lambda_i H| = QP_i$ to $|\lambda_f H| = QP_f$. In a practical measurement the central angle $2\theta_0$ is chosen so that the range $QP_i - QP_f$ is approximately centered about the wanted characteristic wavelength defined by $|\lambda_0 H| = QP_0$.

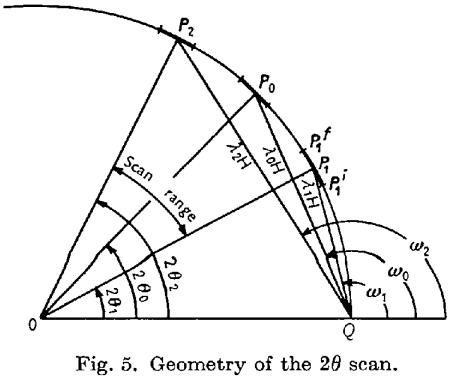

Fig. 5. Geometry of the 2θ scan.

Fig. 5 illustrates the 2θ-scan geometry. For clarity the angular orientation range of the crystal, $\delta\omega$, is not indicated for each of the three crystal orientation angles ω_1, ω_0, and ω_2, but the reader is asked to keep in mind its presence. With the crystal set at the orientation angle ω_1 and the receiving aperture set at the angle $2\theta_1$, the scan across the reflection (hkl) is begun. At the crystal position ω_1 the counter is receiving diffracted intensity from the planes (hkl) due to a band of wavelengths extending from $|\lambda H| = QP_1^i$ to $|\lambda H| = QP_1^f$ and centered about the wavelength $|\lambda_1 H| = QP_1$. At the crystal orientation ω_0 the counter is receiving from the planes (hkl) a band of X-ray wavelengths centering about λ_0, the desired characteristic wavelength. Finally, at the completion of the scan, X-rays of wavelengths centering about λ_2 are being counted with the crystal set at the angle ω_2 and the receiver at $2\theta_2$. During the scanning process the receiver has resolved through the angle $\Delta 2\theta = 2\theta_2 - 2\theta_1$ while the crystal has rotated through one-half this angle,

$$\Delta\omega = \omega_2 - \omega_1 = \tfrac{1}{2}\Delta 2\theta\ .$$

This description of the scanning process has taken no account of any X-ray intensity received by the counter due to wavelengths diffracted by planes other than the specific planes (hkl). In most instances such contributions are of only minor importance, but occasionally they produce significant variations in the background surrounding the point $P(hkl)$ or even changes in the peak intensity. Such effects will be more frequently encountered when the reciprocal lattice translations are small.

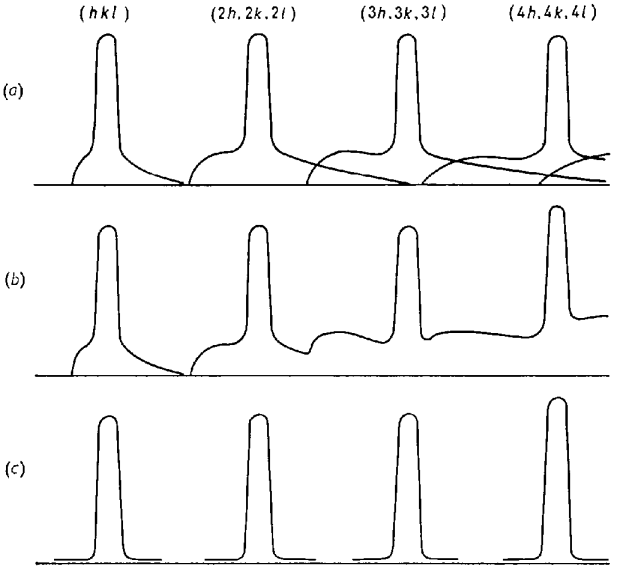

Fig. 6. Hypothetical profiles of the central reciprocal lattice row (nh, nk, nl). (a) and (b) 2θ scan, (c) ω scan.

It has been pointed out that the 2θ-scan follows a central lattice row line. When monochromatization is not complete, as is always more or less true of any actual experiment, every point on the row line has associated with it a linear trail of subsidiary diffracted intensity extending in the direction of the row line. In Fig. 3 this effect has been depicted for any one reciprocal lattice point. In Fig. 6(a) are shown hypo-

thetical spectral profiles associated with the first four members of the central row line (*nh*, *nk*, *nl*). Because

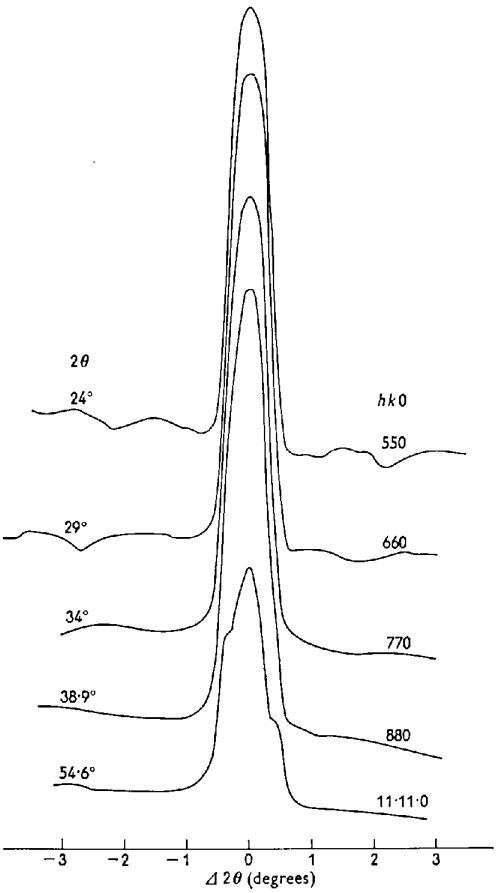

Fig. 7. Experimental profiles of the central reciprocal lattice row (*nh*, *nk*, 0). Tetraphenyl tin, Nb-filtered Mo radiation, 2θ scan.

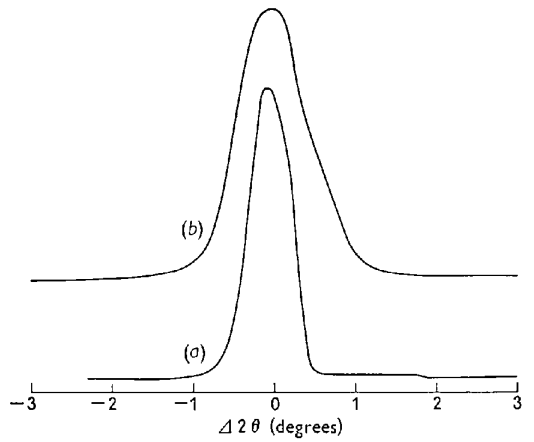

Fig. 8. Experimental profiles obtained with Ni-filtered Cu radiation by the 2θ-scan technique.

(*a*) $(C_6H_5)_2SiCH_2CH_2Si(C_6H_5)_2$, $2\theta = 25{\cdot}2°$.
O

(*b*) $(C_6H_5)_4Si$, $2\theta = 122{\cdot}3°$.

of the increase in dispersion with order n, the spectra overlap to an increasing extent with increasing n. In general, as shown in Fig. 6(*b*), this results in obvious 'background' variations at the lower orders but relatively smooth backgrounds at the higher orders when intensities are measured by the 2θ-scan method. Fig. 7 illustrates this effect by means of five reflections of the sequence (*hk*0) obtained from a crystal of tetraphenyl tin using niobium-filtered molybdenum radiation. Fig. 8 shows the reflection profiles obtained with nickel-filtered copper radiation from two organosilicon compounds at $2\theta = 25{\cdot}2°$ and $122{\cdot}3°$. Compared with the molybdenum patterns the background with copper radiation is seen to be smoother at both small and large angles.

Returning to the ω-scan procedure, as described earlier and illustrated in Fig. 4, the receiving aperture remains stationary at some angle $2\theta_0$ centered about a crystal reflection position while the crystal is rotated through its reflecting angle ω_0, which lies midway between the scan limits ω_1 and ω_2. The result is the same as if the receiver scanned the region of the desired reflection but in a direction transverse to the central lattice row line. As shown in Fig. 6(*c*) the background observed by this technique is lower and much more constant than was obtained using the 2θ-scan technique. This is because the scan path proceeds from a point in reciprocal space completely outside the 'ridge' of general radiation intensity lying in the row line to a corresponding final point on the opposite side of the ridge. It is important to take note of the fact that when the background is measured in this way and subtracted from the over-all intensity including the peak, the net measured intensity of the reflection will contain significant contributions from wavelengths other than λ_0. The unwanted intensity components will tend to bulk largest for unfiltered radiations of short characteristic wavelength and will be at a minimum for crystal-monochromatized radiations including pulse-height discrimination to eliminate submultiples of λ_0.

Fig. 9 shows experimental profiles of the (400) reflection from a crystal of tetraphenyl tin that illustrate the distinctive features of the 2θ and ω scans which were pointed out above. The reader will note the similarity to Fig. 6(*b*) and (*c*). A comparison of the 2θ and ω profiles shows clearly that the lower portion of the ω profile is due to wavelengths in the general radiation spectrum. By interpolating linearily between background readings taken at b_1 and b_2 on the 2θ pattern, one can obtain the integrated intensity due to Mo $K\alpha$ radiation without serious error. This example shows plainly, however, that at small Bragg angles the spectra of the various orders tend to be resolved, necessitating a preliminary mapping of the background surrounding each characteristic reflection. It is self-evident that adopting the practice of measuring the background at points removed some standard distance ($\pm 1{\cdot}5°$ for example) from the peak

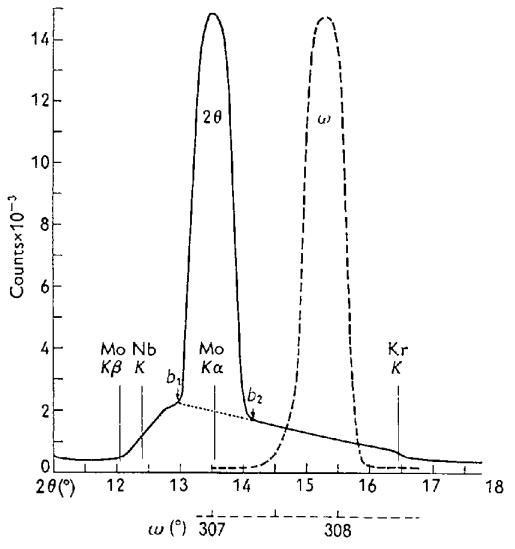

Fig. 9. Experimental profiles of the (400) reflection of $(C_6H_5)_4Sn$ obtained with 2θ and ω scans. Nb-filtered Mo radiation.

position will result not infrequently in significant errors. In Fig. 9 the reader's attention is also directed to the intensity discontinuities caused by the K absorption edges of niobium and krypton. These effects are broad rather than sharp because of the broad X-ray optics of the apparatus.

A more striking example of the contrast between 2θ and ω scans is depicted in Fig. 10. Here the longer

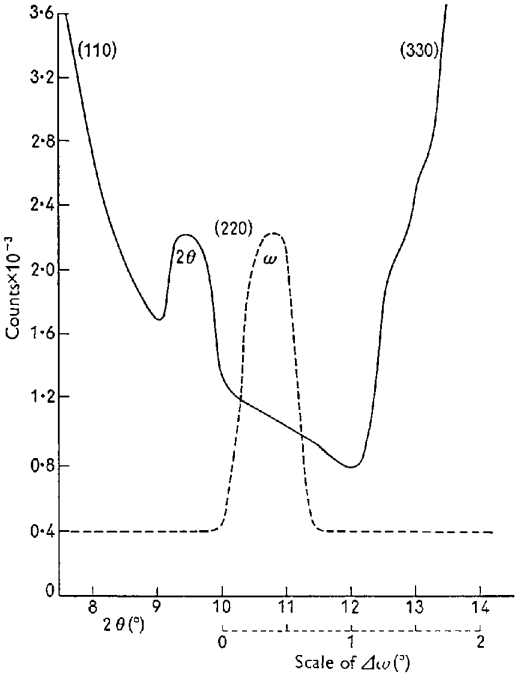

Fig. 10. Experimental profiles of the (220) reflection of $(C_6H_5)_4Sn$ obtained with 2θ and ω scans. Nb-filtered Mo radiation.

wavelengths dispersed by the (110) planes produce a steeply sloping background beneath the feeble (220) reflection. On the contrary, the ω-scan background, although very uniform, would nevertheless lead to a very large positive error in the integrated intensity due to the inclusion of unwanted wavelengths. From the foregoing observations we conclude that the 2θ-scan method lends itself to a proper evaluation of the reflection intensities so long as the intensity profile of the row line concerned is first determined and the scan range judiciously selected for each reflection.

5. Intensity profile of the diffracted beam

We next investigate the nature of the profile of the diffracted beam as a function of displacement of the crystal orientation from the calculated angle ω_0. For simplicity we shall refer to such angular displacements, $\Delta\omega$, as β units. It should be noted that the angular mis-setting of the crystal may also be expressed in terms of $\Delta\theta$ units, which are identical dimensionally with β units. Furthermore, since in the 2θ-scan technique the motions of the crystal and receiver are coordinated with respective velocities $\dot{\omega}$ and $2\dot{\omega}$, the displacement of the receiver from the calculated angle $2\theta_0$ is given by $\Delta 2\theta = 2\beta$.

Attention being confined first to the 2θ-scan procedure, each of the four experimental factors described earlier permits a degree of smearing out of the ideally discrete crystal orientation angle, ω_0, as already explained. Let their intensity profiles as functions of the displacement β be denoted as follows:

spectral dispersion	$I(\beta)_\lambda$
crystal size	$I(\beta)_c$
crystal mosaicity	$I(\beta)_m$
X-ray source	$I(\beta)_x$

These four components combine by the convolution principle, which may be expressed:

$$\begin{aligned} I(\beta)_{\lambda c} &= \int I(\alpha)_\lambda \; I(\alpha-\beta)_c \, d\alpha \,, \\ I(\beta)_{\lambda cm} &= \int I(\alpha)_{\lambda c} \; I(\alpha-\beta)_m d\alpha \,, \\ I(\beta)_{\lambda cmx} &= \int I(\alpha)_{\lambda cm} I(\alpha-\beta)_x \, d\alpha \,. \end{aligned} \qquad (1)$$

If we scan the intensity profile $I(\beta)_{\lambda cmx}$ completely, and assuming that the receiving aperture is large enough to receive the entire diffracted beam, we obtain a measure of the integrated intensity,

$$I_i = \int I(\beta)_{\lambda cmx} d\beta \,, \qquad (2)$$

in which expression we have for simplicity assumed a zero 'background' level. If we want to measure the peak intensity, I_p, we must rotate the crystal until the profile of the convolution $I(\beta)_{\lambda cm}$ superposes the $I(\beta)_x$ profile so as to yield a maximum value of the sum of the products of their respective ordinates. Thus

$$I_p=[I(\beta)_{\lambda cmx}]_{\max}=\left[\int I(\alpha)_{\lambda cm}I(\alpha-\beta)_x d\alpha\right]_{\max}. \quad (3)$$

We now proceed to synthesize the diffracted beam profile $I(\beta)_{\lambda cmx}$ for representative and somewhat idealized components I_λ, I_c, I_m, and I_x. Although the precise shapes of characteristic X-ray emission lines have not yet been determined because of unusual difficulties affecting the experimental techniques, we may to a first approximation assign to the spectral dispersion function a Cauchy shape (Ladell, Parrish & Taylor, 1959), namely,

$$I(\lambda-\lambda_0)=K/[1+(\lambda-\lambda_0)^2/(\tfrac{1}{2}w_\lambda)^2], \quad (4)$$

in which w_λ is the full width at half-maximum intensity of the given spectral line, say, $K\alpha_1$ or $K\alpha_2$. In terms of the angular misorientation of the crystal, β, and for Bragg angles not too close to 90°, equation (4) may be written (Ekstein & Siegel, 1949):

$$I(\beta)_\lambda=K/[1+(2\beta/W_\lambda)^2]. \quad (5)$$

Since when $\beta=0$, $I(\beta)_\lambda=I_{\max}=K$, (5) becomes

$$I(\beta)_\lambda=I_{\max}/[1+(2\beta/W_\lambda)^2]. \quad (6)$$

In equations (5) and (6) W_λ is the full width at half-maximum intensity of the $I(\beta)_\lambda$ profile,

$$W_\lambda=(\Delta\lambda/\lambda)\tan\theta. \quad (7)$$

Compton & Allison have tabulated values of the constant $\Delta\lambda$ for each of the common characteristic radiations (Compton & Allison, 1935, p. 745).

It is shown in Appendix A that the crystal size function for a transparent cylindrical crystal of radius r_c has the intensity profile

$$I(\beta)_c=I_{\max}[1-(R_x\beta/r_c)^2]^{\frac{1}{2}}, \quad (8)$$

where R_x is the distance from the midpoint of the X-ray source to the center of the crystal. We shall assume that mosaic structure of the crystal to be characterized by a Gaussian distribution of orientations. Then

$$I(\beta)_m=K\exp(-k^2\beta^2),$$

where k is determined by the full width at half-maximum intensity,

$$W_m=2\beta_{\frac{1}{2}}=2/k\,(\log_e 2)^{\frac{1}{2}}. \quad (9)$$

When $\beta=0$, $I(\beta)_m=I_{\max}=K$. Hence

$$I(\beta)_m=I_{\max}\exp(-k^2\beta^2). \quad (10)$$

As explained in Appendix B, an acceptable idealized model of the intensity profile of the X-ray source is a trapezoid with the dimensional proportions $\beta_{\frac{1}{2}}/\beta_0=0{\cdot}80$.

Fig. 11 shows the four idealized components of the final intensity profile corresponding to the following specific experimental conditions:

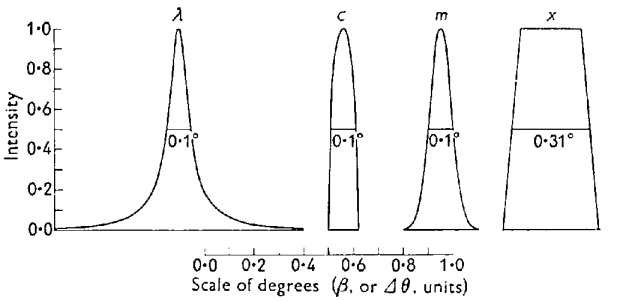

Fig. 11. Idealized components of the final intensity profile for representative experimental conditions: Spectral λ, crystal cross section c, mosaicity m, X-ray source x.

$I(\beta)_\lambda$, spectral profile of the Cu $K\alpha_1$ line with W_λ of equation (6) equal to 0·1°. This is equivalent to $\theta=78°$ using equation (7) with $\Delta\lambda/\lambda=0{\cdot}000378$ (Furnas, 1957).

$I(\beta)_c$, crystal size profile with $r_c=0{\cdot}015$ cm. and $R_x=14{\cdot}55$ cm. in equation (8).

$I(\beta)_m$, crystal mosaicity profile with $W_m=0{\cdot}1°$ as defined by equation (9).

$I(\beta)_x$, trapezoidal X-ray source profile of 0·31° width at half-maximum intensity ($W_x=2\beta_{\frac{1}{2}}=0{\cdot}31°$). This is equivalent to a 'rectangular' focal spot 11 mm. in length at half-maximum intensity, a take-off angle of 4°, and $R_x=14{\cdot}55$ cm.

In Fig. 12 these four components have been combined by the convolution method with the aid of an I.B.M. 650 computer, as indicated in principle in equations (1), to give the final kinematic intensity profile appropriate to the 2θ-scan technique, $I(\beta)_{\lambda cmx}$. Two features of this profile are noteworthy. First, its width at half-maximum intensity, 0·345°, is only slightly greater than that of its broadest component, the X-ray source profile. Second, the slow decay with increasing β of the Cauchy spectral function produces a like extended 'tailing off' of the convolution.

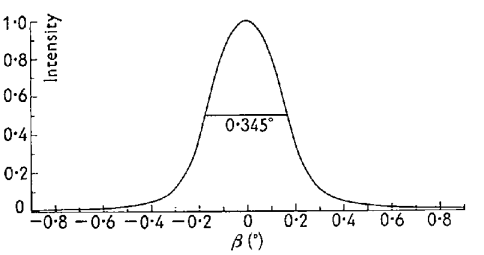

Fig. 12. Kinematic intensity profile, $I(\beta)_{\lambda cmx}$. This is the convolution of the components shown in Fig. 11.

For intermediate take-off angles the dominant influence of the source on the experimental profile is illustrated in Fig. 13. Here the (100) reflection from a small crystal of α-quartz observed at $2\theta=20{\cdot}9°$ using nickel-filtered Cu radiation and a take-off angle of 4° is compared with a synthetic intensity profile

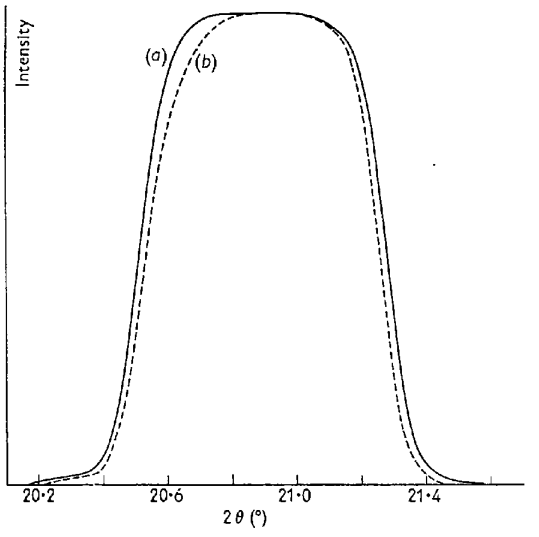

Fig. 13. (*a*) Experimental profile of the (100) reflection of α-quartz. (*b*) Synthetic $\alpha_1\alpha_2$ profile composed of overlapping images of the X-ray source. Cu target, 4° take-off angle, $2\theta = 20{\cdot}9°$.

constructed by superposing two source profiles of the same X-ray tube so as to simulate the $\alpha_1\alpha_2$ composite diffraction image. This was done by displacing a source profile of amplitude 0·5 by an angle 0·054° from an identical profile of amplitude 1·0. It is evident that the combined effects of spectral dispersion within $K\alpha_1$ and $K\alpha_2$, crystal size, and mosaicity modify the source image to only a minor degree. Although the X-ray source is still the dominant component at larger Bragg angles, the effects of spectral dispersion become more conspicuous as can be seen in Fig. 14. Here the (11·7·0) reflection from a crystal of tetraphenyl silicon is compared with a composite $K\alpha_1\alpha_2$ source profile. The diffraction angle is $2\theta = 122{\cdot}3°$ and the separation

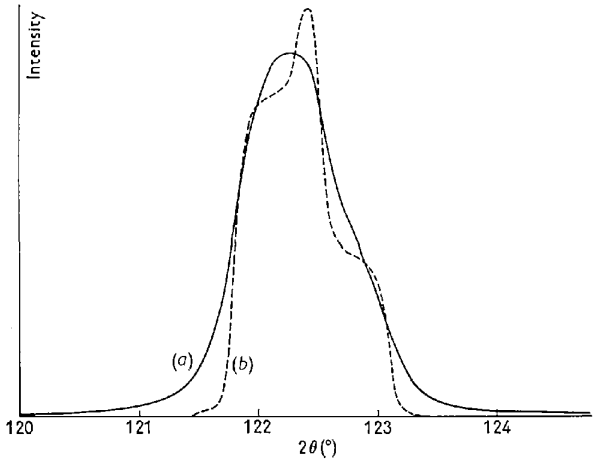

Fig. 14. (*a*) Experimental profile of the (11,7,0) reflection of $(C_6H_5)_4Si$. (*b*) Synthetic $\alpha_1\alpha_2$ profile composed of two overlapping images of the X-ray source. Cu target, 4° take-off angle, $2\theta = 122{\cdot}3°$.

of the Cu $K\alpha$ doublet components is 0·55°. The 'tailing off' of the profile due to the Cauchy-like spectral component is much more noticeable than at $2\theta = 20{\cdot}9°$ (Fig. 13). In addition the experimental profile is considerably smoothed and rounded due to the greater breadth of the spectral element and probably as well to the mosaic character of the crystal.

The slow decay of the spectral component with increasing β results in a continuous decrease in the measured background and increase in the measured integrated intensity as the scan range is increased. This phenomenon is more conspicuous and has more practical consequences at the larger Bragg angles. Fig. 15 portrays by means of a synthesized Cu $K\alpha_{1,2}$ reflection profile for $2\theta = 122°$ how a significant loss in the measured value of I_i will occur for a scan range of 2° Since spectral dispersion varies as $\tan\theta$, the loss in I_i at small θ's is negligible for scanning ranges larger than, say, 2°, whereas at large θ's the losses are appreciable even when using the largest feasible ranges.

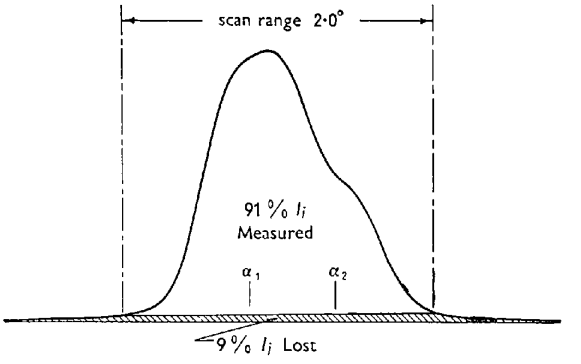

Fig. 15. Loss in measured integrated intensity corresponding to a given scan range. Synthetic Cu $K\alpha_{1,2}$ profile ($I_{\lambda cmx}$) for $W_x = 0{\cdot}31°$ and $2\theta = 122°$.

It is not possible to calculate the extent of the losses in measured values of I_i without a knowledge of the shape of the spectral component, I_λ, of the convolution, $I_{\lambda cmx}$. Double-crystal spectrometer investigations of spectral line shapes do in fact indicate appreciable deviations from the ideal Cauchy shape for β values considerably greater than $\beta_{\frac{1}{2}}$, the abscissa corresponding to half-maximum intensity. Furthermore, it appears that the deviations may differ in both sign and magnitude from one radiation to another, although the results reported to date are too fragmentary to permit a definite conclusion to be drawn (Compton & Allison, 1935, pp. 718–50; Ladell, Parrish & Taylor, 1959)

Bearing in mind the need for clarification of the spectral line shape, we have calculated the losses in the measured values of I_i on the assumption of the Cauchy spectral line shape (equations (4) and (6)) for the typical experimental conditions: $W_c = 0{\cdot}1°$, $W_m = 0{\cdot}1°$, and $W_x = 0{\cdot}31°$ The X-ray source width of 0·31° corresponds to a rectangular focal spot approximately

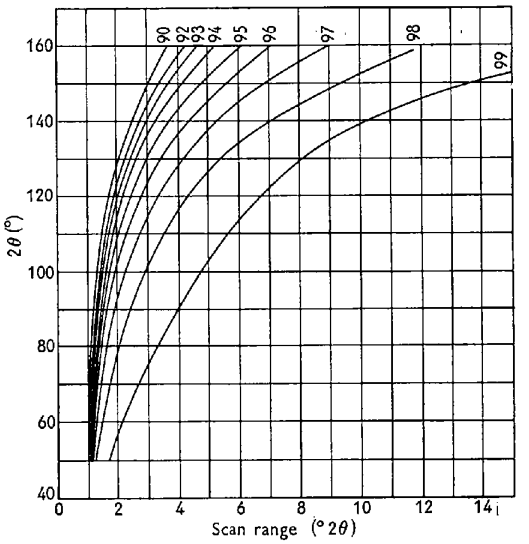

Fig. 16. Measured $\%I_i$ as a function of 2θ and scan range. Experimental parameters: $W_c=0{\cdot}1°$, $W_m=0{\cdot}1°$, $W_x=0{\cdot}31°$, Cauchy spectral profile, Cu $K\alpha$ radiation.

1·0 cm long viewed at a take-off angle of 4·0°. In terms of the convolution notation employed in equations (1), the constant convolution I_{cmx} was first computed and this then convoluted with successive spectral profiles, I_λ, corresponding to the dispersion within $K\alpha_1$ or $K\alpha_2$ for Cu $K\alpha$ radiation at a series of values of 2θ. Finally the effect of $\alpha_1\alpha_2$ separation was allowed for by appropriately displacing one profile $I_{cmx\lambda}$ of intensity 0·5 with respect to a second profile $I_{cmx\lambda}$ of identical shape but unit intensity. These synthetic $(I_{cmx\lambda})\alpha_1\alpha_2$ profiles were then analyzed for $\%I_i$ measured versus scan range in the manner shown graphically in Fig. 15. Fig. 16 shows the results in terms of curves of constant $\%I_i$ measured plotted

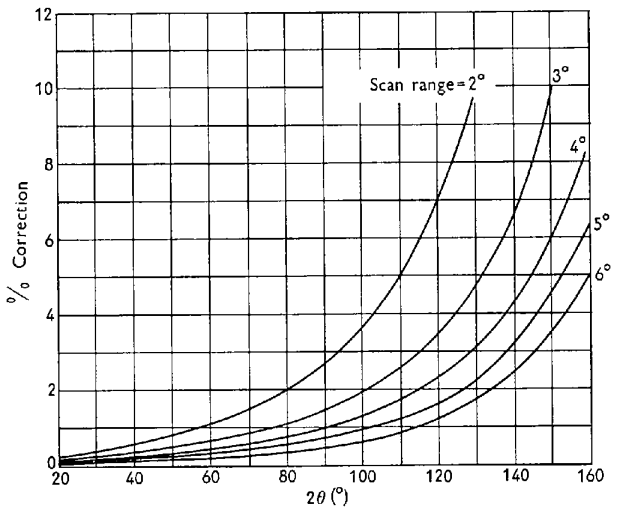

Fig. 17. Corrections to be applied to measured I_i values based on $W_c=0{\cdot}1°$, $W_m=0{\cdot}1°$, $W_x=0{\cdot}31°$, Cauchy spectral profile, Cu $K\alpha$ radiation.

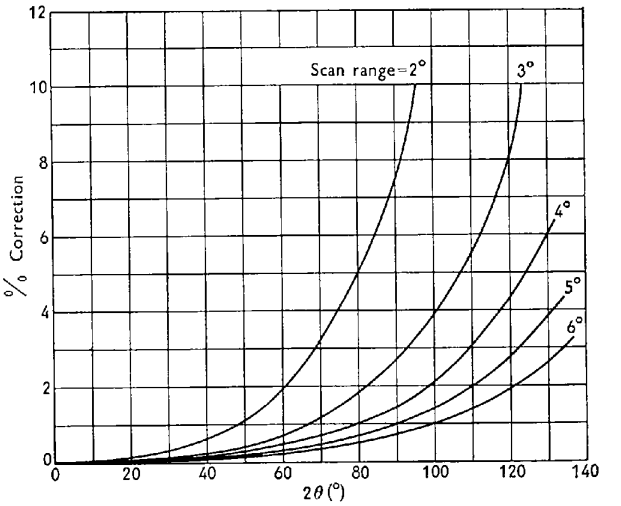

Fig. 18. Corrections to be applied to measured I_i values based on $W_c=0{\cdot}1°$, $W_m=0{\cdot}1°$, $W_x=0{\cdot}31°$, Cauchy spectral profile, Mo $K\alpha$ radiation.

as a function of 2θ and scan range. Fig. 17 portrays the same results in the form of percent corrections to be applied to experimental I_i values for various scan ranges and as a function of 2θ. Fig. 18 gives equivalent correction curves for Mo $K\alpha$ radiation deduced by the same method.

The curves of Figs. 17 and 18 may be used to give first-order corrections to observed measurements of I_i provided their limitations are duly recognized. First and foremost, they are based and sensitively dependent upon a hypothetical spectral line shape for which there is as yet no conclusive experimental evidence. Second, these curves are valid only if the X-ray source width is approximately 0·31° (say within the limits 0·28° to 0·34°) and if W_c and W_m are much smaller than W_x. Hence, for unusually large crystals or for crystals of large mosaic character the curves will be inapplicable.

6. Integrated versus peak intensity

We are now in a position to examine critically the proposition that under appropriate conditions the intensity diffracted by a stationary crystal is proportional to the integrated intensity, which is the same as stating that expressions (2) and (3) are related by a constant factor. In this connection we may observe that (3) is the maximum ordinate of the integrated intensity profile (2).

Because of spectral dispersion, both the angular separation of the $K\alpha$ doublet components and the width of each component are proportional to $\tan\theta$. Furnas has tabulated numerical values of these two effects for the common characteristic radiations (Furnas, 1957). The integral breadth of the pure $K\alpha_1$ or $K\alpha_2$ spectral profile may be expressed:

$$W_\lambda^i = \int I(\beta)_\lambda d\beta / (I(\beta)_\lambda)_{max} = k \tan\theta \,. \qquad (11)$$

But for the purpose of the present discussion $\int I(\beta)_\lambda d\beta$ is constant, which means that the peak intensity, $(I(\beta)_\lambda)_{max}$, varies inversely as $\tan\theta$. Of course the actual intensity profile of a reflection is the convolution of the spectral function I_λ with the other instrumental functions, for which reason the observed decrease in peak intensity and increase in breadth will both be smaller in relative magnitude than those of the pure spectral function. In an earlier publication one of us employed the convolution method to compute the relative broadening of the final convolution in terms of the broadening of one of its elements (Alexander, 1950). Using the same approach we have determined the broadening of the convolution

$$I(\beta)_{\lambda cmx} = \int I(\alpha)_{cmx} I(\alpha-\beta)_\lambda d\alpha$$

as a function of the breadths of its two components, I_{cmx} and I_λ. I_{cmx} was assigned a constant breadth appropriate to a given set of experimental conditions, while the breadth of I_λ was taken to be given by equation (11) with $k=0{\cdot}000378$ (Cu $K\alpha_1$ radiation). The result for representative experimental constants ($W_c=0.1°$, $W_m=0{\cdot}1°$, $W_x=0{\cdot}31°$) is portrayed in I_i/I_p units in Fig. 19 by the curve labeled 'dispersion within α_1 or α_2'. In order to simplify the calculations it has been assumed that the dispersions within α_1 and α_2 are identical, which is only approximately true.

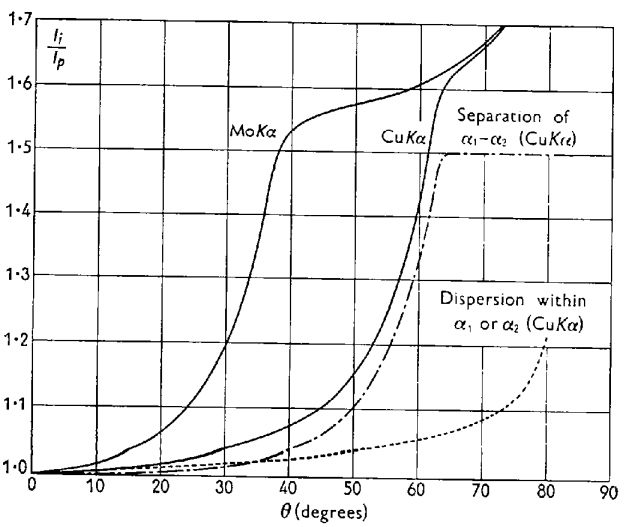

Fig. 19. Calculated dependence of I_i/I_p upon θ due to spectral dispersion effects for Cu $K\alpha$ and Mo $K\alpha$ radiations. $W_x=0{\cdot}31°$, W_c and W_m small with respect to W_x.

Separation of the $K\alpha$ doublet components produces little loss in peak intensity at small Bragg angles because of the extensive overlap of the rather trapezoidal $K\alpha_1$ and $K\alpha_2$ profiles. When, however, the degree of overlap diminishes with increasing θ, the loss in I_p increases rapidly to a limiting value of about 33% for complete resolution. This effect is portrayed for Cu $K\alpha$ radiation and the above-mentioned experimental constants in Fig. 19 by the curve labeled 'separation of $\alpha_1-\alpha_2$'. The over-all increase in I_i/I_p to be expected is given by the product of ordinates of these two spectral dispersion curves, which is the solid curve designated 'Cu $K\alpha$'. The curve marked 'Mo $K\alpha$' was derived by the same procedure using the spectral dispersion parameters characteristic of Mo $K\alpha$ radiation. By expressing I_i/I_p as a function of the ratio of the separation of the $K\alpha$ doublet to the X-ray source width, we can with only minor approximations arrive at a curve which is general for any given radiation (Fig. 20) provided W_c and W_m are small with respect to W_x. One universal curve would be applicable to all radiations were it not that the ratio of spectral width W_λ to angular separation of $K\alpha_1$ and $K\alpha_2$ differs somewhat from one target element to another.

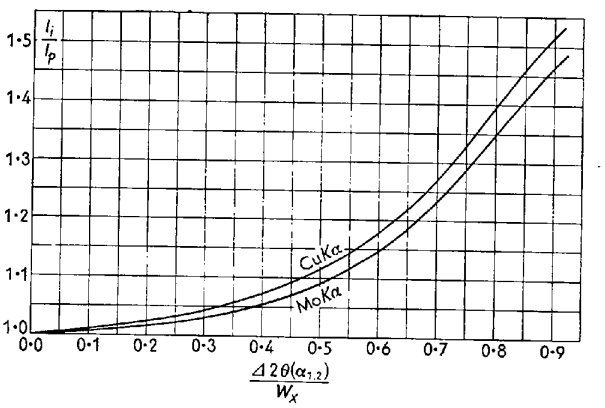

Fig. 20. Calculated dependence of I_i/I_p upon $\Delta 2\theta(\alpha_{1,2})/W_x$ for Cu $K\alpha$ and Mo $K\alpha$ radiations. W_c and W_m small with respect to W_x.

Fig. 21 shows the quality of agreement between the calculated curve for Cu $K\alpha$ radiation and the experimental curves obtained from crystals of four compounds. The observed displacements of the curves of the organo-silicon crystals to the left are due to the presence of more mosaic character, while the shift of the quartz curve to the right is to be expected for less mosaic character, than that incorporated in the calculated curve.

The present results demonstrate plainly that only in a very limited low-θ region can the intensity diffracted by a stationary crystal, I_p, be regarded as approximately proportional to the integrated intensity, I_i (refer to Figs. 19 and 21). Furthermore, because of variations in mosaic character from one crystal to another it is not possible to rely upon any particular calculated curve of I_i/I_p for correcting peak intensities to the equivalent integrated intensities, at least when highly accurate intensities are required. A more dependable approach is to plot a curve of I_i/I_p versus 2θ from 20 or 30 experimental I_i and I_p values for a given crystal, after which the great bulk of the data

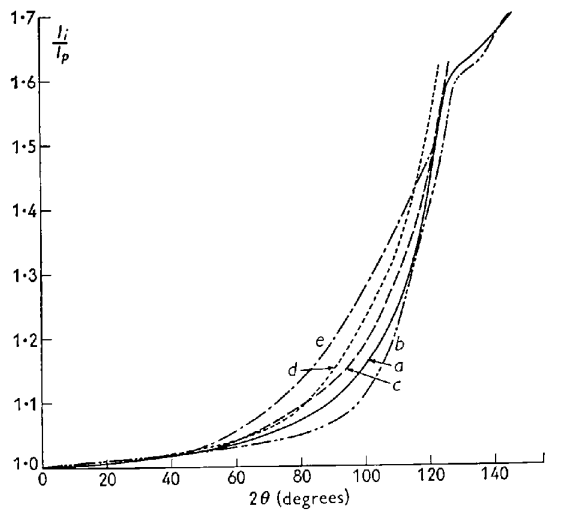

Fig. 21. Comparison of calculated and experimental curves of I_i/I_p for Cu $K\alpha$ radiation. (*a*) Calculated, (*b*) α-quartz, (*c*) $(C_6H_5)_4Si$, (*d*) cyclic tetramer $[(CH_3)_2SiNH]_4$, (*e*) $(C_6H_5)_2SiCH_2CH_2Si(C_6H_5)_2$.

in the form of I_p's can be corrected to the equivalent I_i's with more confidence. If there is pronounced anisotropy of the mosaic character of a given crystal, the application of this method becomes more difficult, but in the authors' experience such cases are the exception rather than the rule. On the other hand, they have commonly observed a monotonic decrease in the diffracting power of a crystal upon prolonged exposure to the X-ray beam, sometimes accompanied by a shift of the I_i/I_p calibration curve.

7. Effects of errors in 2θ, φ, χ, and lattice constants

Errors in alignment of the diffractometer tend to result in approximately constant errors in $2\theta_0(hkl)$ throughout the 2θ scale because of displacement of the 0° point on the goniometer scale from the undeviated beam direction. However, φ_0 depends upon the largely accidental azimuth of the crystal as mounted on the goniometer head; therefore it must be determined experimentally for any given mount. Although the calibration of φ_0 and $\Delta 2\theta_0$ is in principle invariant for a given crystal mount and alignment of the apparatus, it is the authors' experience that these 'constants' drift with the passage of time and require periodic rechecking. Vertical displacements of the center of the crystal or X-ray source from the principal plane of the diffractometer produce calibration errors in χ_0. In Appendix C it is shown that such errors take the form

$$\Delta\chi_0 = C/\sin\theta_0 , \qquad (12)$$

a result which can be easily verified experimentally. After the preliminary alignment of the diffractometer, equation (12) can be used to perfect the alignment of the X-ray source with respect to the equatorial plane of the goniometer. Since for a vertical displacement of this kind $C = t/2R_x$ (see Appendix C), experimental values of $\Delta\chi_0$ and $\sin\theta_0$ for a crystal enable one to compute the vertical displacement t required to bring the source into the equatorial plane of the goniometer.

Any residual displacements of the X-ray source or crystal from the equatorial plane can be dealt with by means of a calibration curve based on equation (12). The constant C is first evaluated from experimental $\Delta\chi_0$ and $\sin\theta_0$ values, after which the required misetting in χ_0 can be deduced for any Bragg angle. The χ profile is relatively broad and flat-topped, and in practice the calibration shows little change with the passage of time; hence any necessary corrections are easily effected.

Serious errors in the measurement of intensities can result from failure to reckon with uncertainties in the knowledge of the lattice constants. For simplicity of illustration we consider the case of an orthogonal unit cell wherein the reciprocal lattice constants are known with the same relative accuracy, $\delta a^*/a^*$. Then

$$\sin\theta = \tfrac{1}{2}\lambda d^* = \tfrac{1}{2}\lambda[(ha^*)^2+(kb^*)^2+(lc^*)^2]^{\frac{1}{2}}$$

and

$$\delta\theta = (3^{\frac{1}{2}}\tan\theta)\delta a^*/a^* . \qquad (13)$$

Both practical experience and a study of theoretical reflection profiles (for example see Fig. 12) show that for $W_x \cong 0{\cdot}3°$ acceptable accuracy in I_p is obtainable only if $\delta\theta$ does not exceed approximately 0·10°. This conclusion applies to the setting of the receiver directly at the calculated $2\theta_0$ for each reflection without resorting to any empirical procedure for refining the 2θ and φ settings.

Table 1. *Values of $\delta\theta$ in degrees for a number of values of θ and $\delta a^*/a^*$*

(Orthogonal unit cell with all three lattice constants known with the same relative accuracy)

	$\delta a^*/a^*$				
θ	0·010	0·005	0·001	0·0005	0·0001
5°	0·087	0·043	0·009	0·004	0·001
10	0·175	0·087	0·018	0·009	0·002
20	0·361	0·181	0·036	0·018	0·004
30	0·573	0·287	0·057	0·029	0·006
45	0·992	0·496	0·099	0·050	0·010
60	1·719	0·859	0·172	0·086	0·017
75	3·704	1·852	0·370	0·185	0·037

Table 1 gives values of $\delta\theta$ in degrees corresponding to five grades of accuracy in the knowledge of $\delta a^*/a^*$ and for a range of values of θ. On the basis of the criterion that $\delta\theta \leqq 0{\cdot}10°$ for intensity measurements of acceptable accuracy, one must not work in the region below and to the left of the broken line. We may observe that in present-day structural investigations of acceptable accuracy $\delta a^*/a^*$ falls in the range 0·003 to 0·0005, which is clearly not good enough to

yield reliable intensities at the larger Bragg angles. The conclusions apply specifically to I_p measurements and somewhat less rigorously to I_i measurements. For non-orthogonal crystal systems the reliability of the intensity measurements is even more sensitively dependent upon the accuracy with which the interaxial angles are known. For the foregoing reasons it is evident that designers of automatic diffractometers must deal effectively with timewise drifts in the instrumental calibrations φ_0 and $\Delta 2\theta_0$, while at the same time users must provide highly accurate lattice constants.

8. Practical recommendations: 2θ-Scan technique for measuring integrated intensities

Initial choice of instrumental conditions

(1) Determine at least approximately the ratio R_x/R_z of the apparatus. As explained in Appendix D, there are some advantages in making this ratio unity.

(2) As a general rule the take-off angle of the X-ray beam may be chosen so that the projected focal spot is approximately equidimensional. This is about 4° for conventional rectangular focal spots viewed longitudinally. The equivalent vertical and horizontal angular dimensions, α_x^v and $\alpha_x^h(=\gamma_x)$, may be determined from a pinhole image.

A wider projected focal spot (larger take-off angle) has both advantages and disadvantages, which must be weighed in any particular case. The advantages include: (*a*) the 2θ region of approximate proportionality of I_i and I_p is extended (Figs. 19 and 21), (*b*) less precision is required in the setting of θ in order to obtain acceptable accuracy in I_p (Section 7 and Table 1), and (*c*) the minimum angle of resolution of the $K\alpha$ doublet is increased.

The disadvantages are: (*a*) the peak intensity is reduced, (*b*) the scan range must be increased, and (*c*) a larger receiving aperture is needed.

(3) Determine the limiting crystal dimension, $l_c=\gamma_c R_x$, as governed not only by the linear absorption coefficient but also by the values of γ_R, γ_x, γ_m, and R_x, R_z. For ordinary experimental conditions refer to equation (D·9) and Fig. 34.

(4) If γ_R is adjustable, it should be made sufficiently large to allow for possible mosaicity of the crystal (for example, let $\gamma_m=0{\cdot}45°$) as illustrated in Fig. 34. Ordinarily $(\gamma_R)_{\min}$, the minimum receiving aperture width, should not be less than 2°. For exceptionally mosaic crystals it may be necessary to construct a receiving collimator with an abnormally large aperture, which, of course, must be employed in conjunction with a counter window of the same or larger angular aperture. In extreme cases it may be necessary to employ the ω-scan technique in order to obviate the aperture difficulty (see equations (D·10) and (D·11)). Practical techniques for measuring the mosaic spread of a crystal are described by Furnas (1957, pp. 138–9).

(5) If γ_R and R_x/R_z of the apparatus are invariant, it may be necessary to more sharply restrict γ_c and γ_x according to the limitations established by equation (D·9).

(6) Other considerations being equal, it is advantageous to employ a short wavelength in order to avoid making intensity measurements in the high 2θ region where scan range corrections become unreliable. For a more extensive treatment of this subject see Furnas, 1957, pp. 26–27.

Technique of measurement

(1) At best, corrections for intensity losses due to finite scan range are only approximate. Therefore, when the diffraction pattern is almost entirely confined to the region $2\theta<90°$, either by virtue of the choice of wavelength or the thermal vibrational amplitudes of the atoms, or both, it can be seen from Figs. 17 and 18 that the correction can be neglected with impunity provided the scan ranges employed are not too small.

(2) At the lower Bragg angles, and particularly when using a radiation of short wavelength such as Ag $K\alpha$ or Mo $K\alpha$, it is necessary to make a preliminary map of the background surrounding each reflection in order to avoid serious errors resulting from an unwise choice of the scan range and locations of background measurements. In this connection refer again to Figs. 6, 7 and 9. At very small θ's the determination of the background becomes difficult because the characteristic background profile due to general radiation contracts to such an extent on the 2θ scale as to largely disappear within the main reflection profile, the width of which is principally due to the X-ray source (see Fig. 13). Under these circumstances the authors have found the I_i/I_p curve of the crystal in question to be invaluable for the purpose of revealing an incorrect determination of the background by virtue of the fact that the reflection concerned tends to deviate from the established curve.

APPENDIX A

Diffraction of monochromatic X-rays from a point source by a small perfect crystal

We seek the answers to four main questions. When the crystal rotates through its entire angular range of reflection $-\beta$ to $+\beta$,

(1) Does diffraction occur from the entire volume of the crystal?
(2) What is the angular retardation, $\Delta\beta$, of diffraction from non-equatorial sections of the crystal?
(3) What is the intensity profile, $I(\beta)_c$, of the diffracted radiation?
(4) What is the range of solid angle in which diffracted rays occur?

We assume the following crystal model: a cylinder of radius r_c and length l, transparent to the incident X-rays of wavelength λ_0, perfect (no mosaic character). The crystal C is uniformly irradiated with X-rays of wavelength λ_0 originating from the point source X (Fig. 22). If unit volume of the crystal diffracts X-rays from planes (hkl) with intensity I_0, the integrated intensity may be defined by:

$$I(hkl)_t = I_0 \iiint dx\,dy\,dz$$
$$= I_0 V ,$$

V being the volume of the crystal.

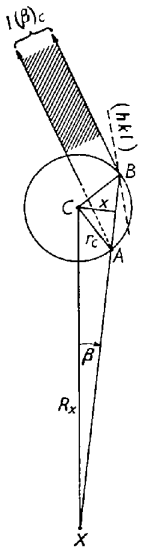

Fig. 22.

Consider first diffraction from an equatorial section of the crystal as shown in Fig. 22. When the crystal is rotated to some azimuthal angle ω_0 about the cylindrical axis, the central ray CX makes the Bragg angle with the planes (hkl). If now the crystal is turned slightly to the angle β, the incident ray XAB fulfills the Bragg condition with these same planes but along the line AB, generating a plane sheaf of diffracted rays of total intensity $I(\beta)_c$ as indicated by the hatched zone of the figure. The intensity is proportional to the length of the chord AB,

$$I(\beta)_c = 2k(r_c^2 - x^2)^{\frac{1}{2}}$$
$$= 2k(r_c^2 - R_x^2\beta^2)^{\frac{1}{2}}.$$

For the central ray $\beta = 0$ and $I = I_{\max}$, so that

$$I(0)_c = I_{\max} = 2kr_c .$$

Therefore we obtain for the profile of the diffracted rays:

$$I(\beta)_c = I_{\max}\,[1 - (R_x\beta/r_c)^2]^{\frac{1}{2}} . \qquad (A\cdot1)$$

Finite diffracted intensity is obtained between the crystal orientation limits $\beta = \pm r_c/R_x$ radians. During the rotation of the crystal through this angular range, the diffracted rays extend over an interval on the 2θ scale which is a function of 2θ and the relative sizes of R_x, R_z, and r_c. However this interval is at a maximum when 2θ approaches zero. From Fig. 23 it can be seen that its maximum extent is then

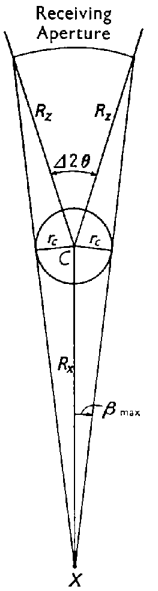

Fig. 23.

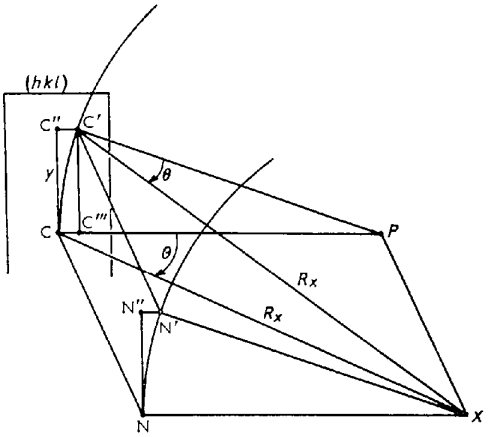

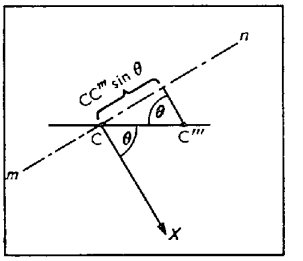

Fig. 24.

$$\Delta 2\theta = (2r_c/R_x).([R_x+R_z]/R_z) = 2r_c([R_x+R_z]/(R_xR_z)) . \quad (A\cdot2)$$

In concluding this treatment of diffraction by the equatorial section of the crystal, we may make the observation that as the crystal turns through its angular reflecting range, $-r_c/R_x$ to $+r_c/R_x$ radians, the locus of reflecting points, AB, moves across the entire cross-section of the crystal (Fig. 22). Hence, all points in this section contribute to the integrated reflection intensity.

We now consider diffraction from the planes (hkl) at points in the crystal removed from the equatorial section. Referring to Figs. 22 and 24, we see that when the incident equatorial ray XC fulfills the Bragg condition, the equivalent point C'' at height y does not diffract. However, the neighboring point C' at height y does diffract since the ray XC' is incident upon the planes (hkl) at the Bragg angle. Thus diffraction at height y occurs simultaneously with diffraction on the equator except that there is a linear displacement of $C'C''$. This displacement is equivalent to an angular retardation $\Delta\beta$ which can be expressed in terms of the experimental parameters y, R_x, and θ. It is useful to employ an approximate expression for the sagitta, $CC''' = C'C''$,

$$CC''' = y^2/(2CP) , \quad (A\cdot3)$$

which is good to within 0·2% for $y/CP < 0{\cdot}09$. The component of CC''' projected on a horizontal line mn (see Fig. 24, inset) normal to XC is

$$CC''' \sin\theta = y^2 \sin\theta/(2CP) ,$$

and its angular equivalent subtended at X is

$$\Delta\beta = y^2 \sin\theta/(2R_xR_x\cos\theta) = \tfrac{1}{2}(y/R_x)^2 \tan\theta \text{ radians} . \quad (A\cdot4)$$

Thus we have demonstrated that diffraction from points in a crystal at height y is displaced, or retarded, by the angle $\Delta\beta$ with respect to diffraction from the corresponding points in the equatorial section. If reference is now made to Fig. 25, when diffraction occurs along the line EF in the equatorial section, diffraction is taking place simultaneously along some line $E'F'$ at mean height y, and in fact diffraction is occurring simultaneously throughout the two-dimensional region $EE'F'F$. Finally it follows that during rotation of the crystal through its angular range of diffraction, this diffracting zone sweeps across the entire volume of the crystal. Thus we have answered questions (1) and (2) at the beginning of this appendix.

Questions (3) and (4) have been answered only for the equatorial section. The answer to the vertical aspect of question (4) can be easily given by a consideration of Fig. 26. An incident equatorial ray XC generates a diffracted ray CZ. Since y is very small with respect to R_x we can, for the present purpose, neglect the displacement of the diffracting point C' from its true position ($C''C'$ of Fig. 24) and likewise

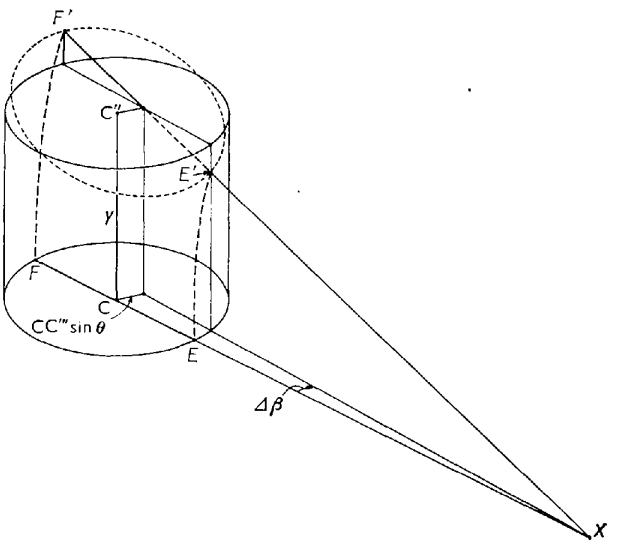

Fig. 25.

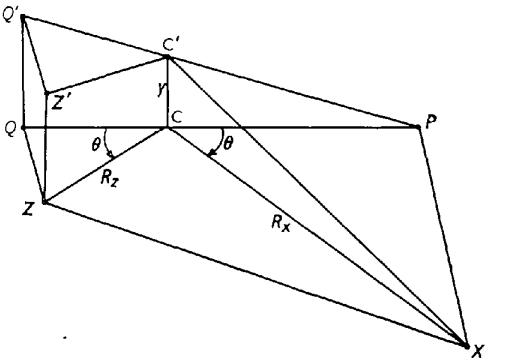

Fig. 26.

regard the terminus of the non-equatorial diffracted ray as falling at Z'. To a very good approximation, then

$$ZZ' = y/R_x.(R_x+R_z) ,$$

and the angle subtended at C is

$$\alpha = ZZ'/R_z = y((R_x+R_z)/(R_xR_z)) , \quad (A\cdot5)$$

which is of the same form as expression (A·2). If h_c is the over-all height of the crystal, the maximum vertical angular extent of the diffracted radiation is then,

$$\alpha_c^v = h_c((R_x+R_z)/(R_xR_z)) . \quad (A\cdot6)$$

Equations (A·2) and (A·6) specify the minimum horizontal and vertical dimensions of the receiving aperture required to encompass the entire diffracted beam from a small perfect crystal of radius r_c and length h_c when the receiver is kept stationary. Of course the angular divergence of the diffracted rays due to experimental factors other than crystal size must also be taken into account in choosing the dimensions of the receiving aperture (see Appendix D).

We must now evaluate the diffraction profile for the entire volume of the crystal. For a circular section on the equator it was found to be given by equation (A·1). To include the contributions from sections at all heights we need to integrate over all values of y, bearing in mind the variation in retardation angle, $\Delta\beta$, with y, or therefore:

$$I(\beta)_v = \int_{-\frac{1}{2}h_c}^{+\frac{1}{2}h_c} I(\beta - \Delta\beta_y)_c dy \,. \qquad (A\cdot7)$$

If $\frac{1}{2}h_c$ is very small with respect to R, the non-equatorial sections may be regarded for practical purposes as circular (even though they are in fact elliptical). Hence, we may substitute in (A·7) expression (A·1) for $I(\beta - \Delta\beta_y)_c$:

$$I(\beta)_v = I_{\max} \int_{-\frac{1}{2}h_c}^{+\frac{1}{2}h_c} \{1 - [R_x(\beta - \Delta\beta_y)/r_c]^2\}^{\frac{1}{2}} dy \,. \quad (A\cdot8)$$

We must now determine the magnitude of the retardations, $\Delta\beta_y$, of the non-equatorial contributions in equation (1·8). Let us evaluate expression (A·4) for a representative range of the parameters y, R_x, and θ. The numerical results are tabulated in Table 2 for $R_x = 10$ cm., $\theta = 30°$, 45°, 60°, and 80°, and y ranging from 0·005 to 0·03 cm. This maximum y value corresponds to a crystal of 0·6 mm. over-all height. Since the present analysis applies only to an apparatus in which the X-ray source dimensions are large with respect to the crystal dimensions, and since actual source heights seldom exceed 1·0 mm., we may conclude that $y_{\max} = 0{\cdot}03$ cm. represents an unusually large value of the crystal height. It will be seen from Table 2 that only for large y's and θ's does the retardation exceed 0·001°. For a more typical y value of 0·015 and somewhat lower Bragg angles it is seen that $\Delta\beta$ is of the order of 0·0001° or less. The significance of these results is more apparent when we consider the equivalent *fractional* retardations. Assigning to the crystal the representative angular width of 0·1°, we find that only at very large values of y and θ does $\Delta\beta$ exceed one-hundredth of this figure. This means that except under very extreme experimental conditions $\Delta\beta_y$ in (A·8) may be neglected and the intensity profile of the cylindrical crystal regarded as not sensibly different from that of its equatorial section, equation (A·1).

Table 2. *Values of the retardation angle $\Delta\beta$ in degrees as a function of y and θ*

($R_x = 10$ cm.)

	θ (degrees)			
y (cm.)	30	45	60	80
0·005	0·00000$_4$	0·00001	0·00002	0·00004
0·010	0·00002	0·00003	0·00006	0·00016
0·015	0·00004	0·00006	0·00014	0·00037
0·020	0·00007	0·00011	0·00026	0·00065
0·025	0·00010	0·00018	0·00040	0·00102
0·030	0·00015	0·00026	0·00058	0·00146

APPENDIX B

Diffraction of monochromatic X-rays from a source of finite dimensions by a vanishingly small, perfect crystal

As in Appendix A we are interested in the answers to four main questions. When the crystal rotates through its entire angular range of reflection $-\beta$ to $+\beta$,

(1) Does the crystal diffract X-rays originating at all points on the source?
(2) What is the angular retardation, $\Delta\beta$, of diffraction generated by rays from non-equatorial sections of the source?
(3) What is the intensity profile, $I(\beta)_x$, of the diffracted radiation?
(4) What is the range of solid angle in which diffracted rays occur?

Because of the close parallelism between the geometry pertinent to this appendix and that of Appendix A, one is inclined to predict without formal proof that the answers to these four questions will likewise be equivalent. This, in fact, turns out to be the case, but still a minimal systematic analysis will be presented in order to guard against possible failure of some aspects of the analogy.

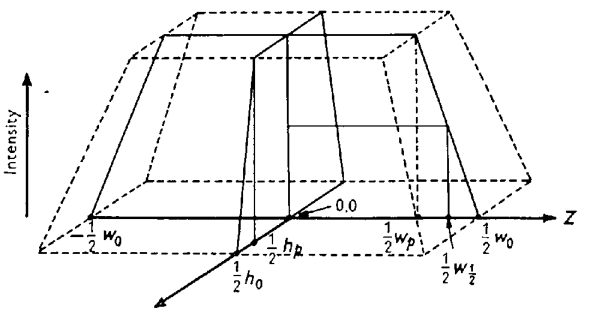

Fig. 27.

An examination of the horizontal intensity profiles of the focal spots of good-quality diffraction tubes shows that they resemble closely somewhat rounded regular trapezoids. We therefore adopt the idealized intensity profile of the projected source shown in Fig. 27, a three-dimensional figure with two mutually perpendicular trapezoidal sections. Although the vertical section is presumed to be trapezoidal, its actual shape is, in fact, of no consequence in the following discussion. Basing our definitions of the vertical and horizontal directions upon the convention that the plane of diffraction (equatorial plane) defines the horizontal plane of the apparatus, the vertical trapezoidal section has full peak and base lengths of h_p and h_0 respectively and the horizontal section peak and base lengths of w_p and w_0 respectively. The angles subtended at the crystal by these horizontal lengths

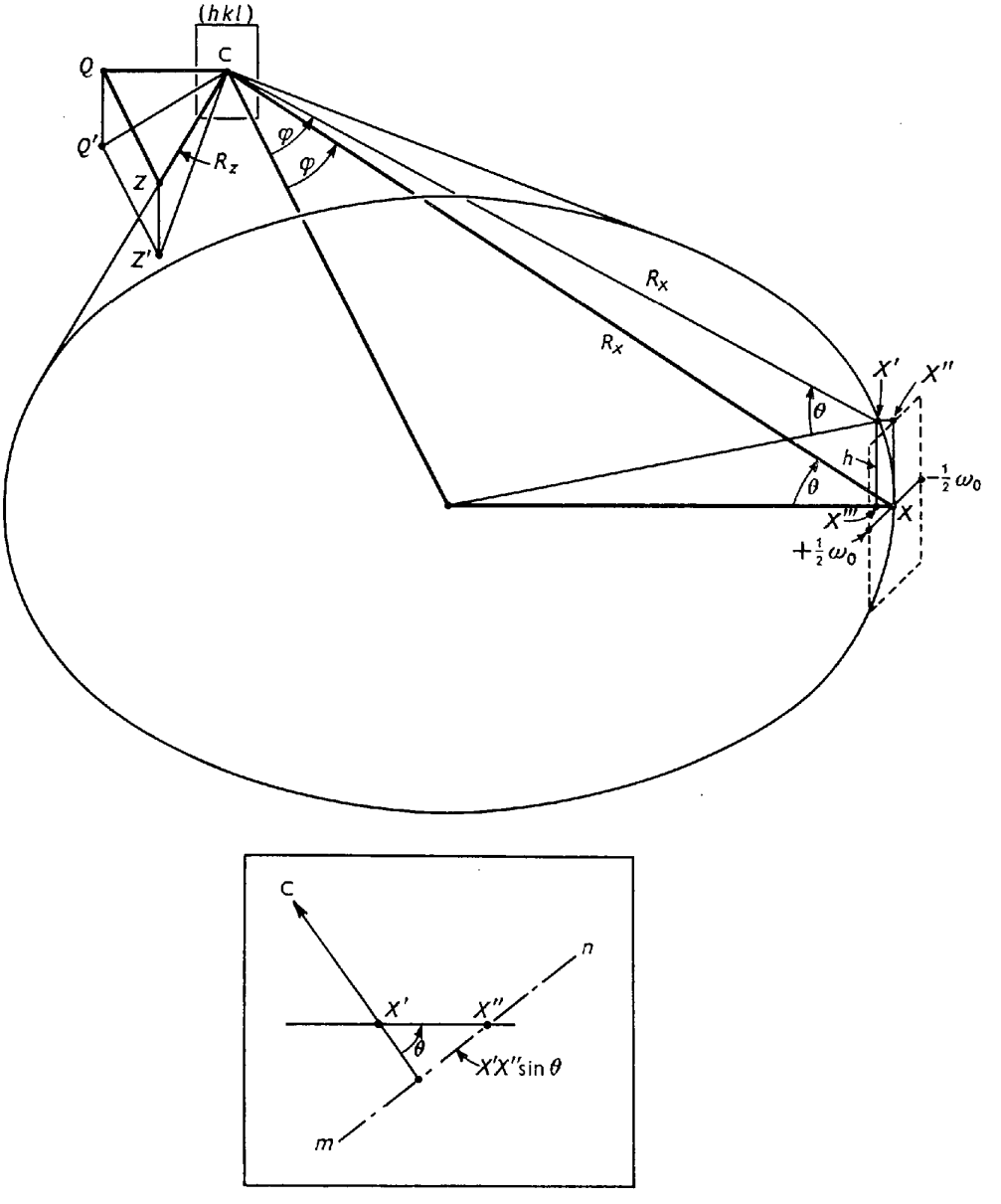

Fig. 28.

are $2\beta_p$ and $2\beta_0$ respectively. We may also define the width at half-maximum intensity, $w_{\frac{1}{2}}$, and its angular equivalent, $2\beta_{\frac{1}{2}}=W_x$. The 'best' trapezoids fitted to the horizontal source profiles of actual X-ray tubes were found to have approximate dimensional proportions as follows: $\beta_p/\beta_0=0{\cdot}60$ and $\beta_{\frac{1}{2}}/\beta_0=0{\cdot}80$.

In the following the reader is asked to refer to Figs. 27 and 28. As the crystal rotates through its reflecting position, diffraction takes place from the planes (*hkl*) successively using incident rays emitted along the equatorial line $-\frac{1}{2}w_0$ to $+\frac{1}{2}w_0$ on the projected focal spot. The profile of the diffracted rays, $I(\beta)_x$, will be an image of the equatorial section of the source. We next consider diffraction from the planes (*hkl*) due to rays emitted from non-equatorial points on the source. At the same time as the central equatorial ray XC fulfills the Bragg condition, the non-equatorial ray $X'C$ from a point at the approximate height h will likewise satisfy the Bragg relation. As the crystal rotates through its reflecting position, rays emitted by successive points along a horizontal path at this same height on the source will produce diffracted rays. It can be seen from Fig. 28 that these observations are only special cases of diffraction by the crystal at the point C due to incident rays originating anywhere on the surface of a cone with semi-apex angle φ and apex C. As the crystal rotates, this cone turns with it and the locus of intersection

of the cone and the source sweeps across the latter. Thus it has been demonstrated that the crystal will diffract X-rays originating at all points on the source (question (1)).

We next evaluate the difference in azimuth, or equatorial angular component, of the two incident rays XC and $X'C$, for which we may refer to Fig. 28. An examination of the geometry of this figure shows that it is similar to that of Fig. 24 if we interchange P for N, C for X, C' for X', etc. Therefore the equatorial angular component is given by an equation of the same form as (A·4):

$$\Delta\beta = \tfrac{1}{2}(h/R_x)^2 \tan\theta \text{ radians} . \qquad \text{(B·1)}$$

It also follows that the angular retardation of diffraction due to non-equatorial zones of the X-ray source has the same properties as those of the retardation of diffraction by the non-equatorial sections of the crystal (Appendix A).

Numerical values of the retardation angle $\Delta\beta$ will, of course, be the same as those given in Table 2. However, since the full angular width of the focal spot is of the order of $2\beta_0 = 0{\cdot}6°$ rather than $0{\cdot}10°$ as in the case of the crystal cross-section, the *fractional* retardation angles will be much smaller in the present case. So we conclude immediately that the retardation of diffraction by the non-equatorial rays is negligible for practical purposes, and, therefore, the intensity profile of the source measured as a function of β by a receiver of sufficient aperture is the same as the equatorial profile.*

We have now to specify the horizontal and vertical angular ranges within which diffracted rays occur. If the over-all width of the source profile is w_0, as for the idealized source profile of Fig. 27, then the horizontal angular range subtended at the crystal is w_0/R_x and the range subtended by its diffraction image will be the same. Referring to Figs. 27 and 28, in the same manner, if the over-all height of the source is h_0, the vertical angular range of the incident rays is h_0/R_x and that of the diffracted rays will be equal:

$$2ZZ'/R_z = h_0/R_x . \qquad \text{(B·2)}$$

These angular ranges must be used in the process of calculating minimal receiver apertures (refer to Appendix D).

APPENDIX C

Relationship among $\Delta\chi$, θ, and the receiving aperture height

As shown in Fig. 29, when planes (hkl) are oriented vertically so that the incident equatorial ray XC satisfies the Bragg relation, a diffracted ray is generated in the direction CT in the equatorial plane. If the crystal is tilted about the χ axis from the calculated angle χ_0 by an amount $\Delta\chi$, as indicated in the drawing, an incident ray $X'''C$ from the equator of the X-ray source now satisfies the Bragg relation with the same planes, generating a diffracted ray in the direction CT'''. Let $Z''Z'''$ be the elevation of this diffracted ray at the receiving aperture, which is a distance R_z from the crystal. With sufficient exactness the angular displacement of the diffracted ray is then $\alpha = Z''Z'''/R_z$. From Fig. 29 it can be seen that with the planes (hkl) tilted to the angle $\Delta\chi$, incident X-rays lying anywhere on the surface of a cone of semi-apex angle φ and terminating at C will satisfy the Bragg relation and generate diffracted rays.

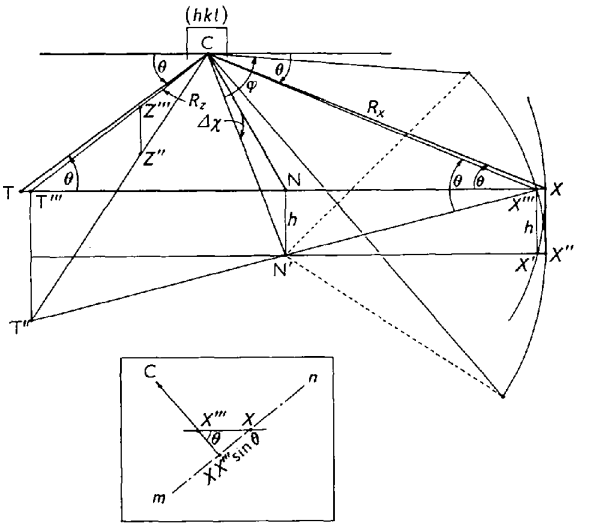

Fig. 29.

From an inspection of the figure we see that

$$\tan\Delta\chi = (NN'/CN) = (NN'/R_x \sin\theta) . \qquad \text{(C·1)}$$

Furthermore

$$NN' = X'''N'(T'''T''/X'''T'') = \tfrac{1}{2}(T'''T'') ,$$

and to a sufficiently good approximation for small values of $\Delta\chi$:

$$T'''T'' = Z'''Z''(R_x/R_z) .$$

It follows that

$$\begin{aligned}\tan\Delta\chi &= \tfrac{1}{2}Z'''Z''(R_x/R_z).1/(R_x\sin\theta)\\ &= \tfrac{1}{2}Z'''Z''/(R_z\sin\theta)\\ &= \alpha/(2\sin\theta) ,\end{aligned}$$

where α is the angular displacement of the diffracted ray from the equatorial plane (compare Furnas, 1957, p. 80). Since in practice $\Delta\chi$ must of necessity be small, we make negligible error in saying

$$\alpha = 2\Delta\chi \sin\theta . \qquad \text{(C·2)}$$

* Actually this statement is not completely valid because some distortion is introduced into the 'ideal' horizontal profile as a result of the non-rectangular profile of vertical sections of the X-ray source. However the degree of distortion will be small and of little practical consequence.

Since $\alpha_{\max}$ may be regarded as defined by one-half the receiving aperture height, (C·2) is the desired equation relating this parameter to $\Delta\chi$ and θ. It states that for a given receiving aperture the width of the χ profile of a diffracted beam will vary as $1/\sin\theta$.

The X-ray source height likewise establishes a limiting value of $\Delta\chi$. The analysis takes a form identical with that just outlined for the receiver height, so that

$$\alpha_x = 2\Delta\chi \sin\theta ,$$

α_x being one-half the angular equivalent of the source height. The limiting value of $\Delta\chi$ as governed by the combined effect of the receiver, source, and mosaic range of the crystal, γ_m, is therefore

$$\Delta\chi_{\max} = ((\alpha_r + \alpha_x)/2 \sin\theta) + \tfrac{1}{2}\gamma_m , \qquad (C·3)$$

where α_r is one-half the angular equivalent of the receiving aperture height. In actual practice α_x is much smaller than α_r, so that the receiving aperture height plays the dominant role unless the mosaic spread of the crystal is large. We may also note that $\alpha_m = \gamma_m \sin\theta$.

It is of interest to evaluate the angular equatorial displacement of the incident ray, XC, corresponding to a given angular displacement of the diffracted ray from the equatorial plane. Because of the smallness of practicable values of $\Delta\chi$, we may neglect the non-coplanarity of the two circles of radius $NX = N'X''$ with centers at N and N', as suggested by the geometry of Fig. 29. The linear displacement along the line XT is XX'''. By the sagitta approximation and other geometrical considerations discussed above, we make little error in saying:

$$XX''' = (NN')^2/2NX = (\tfrac{1}{2}.Z'''Z''.(R_x/R_z))^2/(2R_x \cos\theta)$$
$$= \alpha^2 R_x/(8 \cos\theta) .$$

Referring to Fig. 29 and Fig. 29 (inset), we see that the angular equivalent of the displacement XX''' is:

$$\beta_{XX'''} = XX''' \sin\theta/R_x = \tfrac{1}{8}\alpha^2 \tan\theta . \qquad (C·4)$$

Supposing that $\alpha = 1°$, for example, we find that $\beta_{XX'''} = 0·0022 \tan\theta$ degrees. This shows that for experimentally meaningful values of α the horizontal displacement of the incident ray from the midpoint of the focal spot is small compared with the over-all angular width of the focal spot itself, which is of the order of 0·3–0·6° for the technique under consideration.

Another practical problem can be answered in terms of the geometry of Figs. 29 and 30. If the midpoint of the X-ray source is displaced from the equatorial plane of the diffractometer, what will be the resulting displacement of the intensity profile on the χ scale? With reference to Fig. 30, let XCT be the equatorial plane and let the incident ray XC from the midpoint X of the source produce a diffracted ray CT from planes (hkl) of a point crystal at C. CN is the normal to the diffracting planes. The full vertical height of the receiving aperture is Z_1Z_1', equivalent to the angular aperture $\alpha^v = Z_\perp Z_\perp' R_z$.

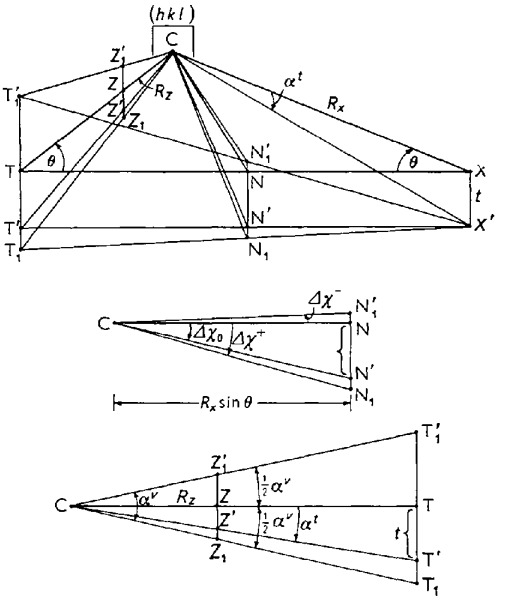

Fig. 30.

Suppose now the X-ray source is displaced vertically by the amount $XX' = t$, which is very small in comparison with R_x (Fig. 30). We wish to determine the angular displacement of the midpoint of the χ intensity profile. The upper and lower limits of χ are determined respectively by the limits Z_1 and Z_1' of the receiving aperture. As seen from the figure, with reference to the midpoint X' of the displaced source these limits correspond to the diffracted rays CT_1 and CT_1' and to the plane normals CN_1 and CN_1' respectively. The equivalent values of $\Delta\chi$ are $\Delta\chi^+$ and $\Delta\chi^-$, and the angular displacement of the midpoint of the χ profile from the equatorial section is then

$$\langle\Delta\chi\rangle = \tfrac{1}{2}(\Delta\chi^+ - \Delta\chi^-) . \qquad (C·5)$$

We now proceed to evaluate $\Delta\chi^+$ and $\Delta\chi^-$. With reference to Fig. 30, since t is very small relative to R_x, we may to a very good approximation regard $X'CT'$ as the temporary (equatorial) plane of reference and employ the geometry of Fig. 29 and equation (C·2) to express the angular displacements of the diffracted rays CT_1 and CT_1' from the reference ray CT'. For ray CT_1 we obtain

$$\tfrac{1}{2}\alpha^v - \alpha^t = 2(\Delta\chi^+ - \Delta\chi_0) \sin\theta , \qquad (C·6)$$

and for ray CT_1'

$$\tfrac{1}{2}\alpha^v + \alpha^t = 2(\Delta\chi^- + \Delta\chi_0) \sin\theta . \qquad (C·7)$$

Subtraction of (C·7) from (C·6) gives

$$-2\alpha^t = 2(\Delta\chi^+ - \Delta\chi^- - 2\Delta\chi_0) \sin\theta ,$$

and then

$$\langle \Delta\chi \rangle = \tfrac{1}{2}(\Delta\chi^+ - \Delta\chi^-) = -(\alpha^t/(2\sin\theta)) + \Delta\chi_0 .$$

But

$$\Delta\chi_0 = t/R_x \sin\theta = \alpha^t/\sin\theta ,$$

so that

$$\langle \Delta\chi \rangle = \alpha^t/(2\sin\theta) = t/(2R_x \sin\theta) . \qquad \text{(C·8)}$$

We note from equation (C·8) that the signs of $\langle \Delta\chi \rangle$ and t are the same. Thus a positive (downward) displacement of the X-ray source results in a positive value of $\langle \Delta\chi \rangle$.

APPENDIX D

Dimensions of the receiving aperture

1. *Vertical dimensions*

The minimal receiving aperture dimension is determined by the sum of the over-all vertical divergences of the diffracted rays due to crystal height (α_c^v), X-ray source height (α_x^v), and crystal mosaicity (α_m^v):

$$\alpha^v = \alpha_c^v + \alpha_x^v + \alpha_m^v . \qquad \text{(D·1)}$$

In terms of α_m of Appendix C we note that $\alpha_m^v = 2\alpha_m$. Substituting from equations (A·6) and (B·2) and employing the expression for α_m given in Appendix C, we may write

$$\alpha^v = h_c((R_x + R_z)/(R_x R_z)) + h_x/R_x + 2\gamma_m \sin\theta , \qquad \text{(D·2)}$$

wherein h_c and h_x represent the over-all heights of the crystal and focal spot respectively. For a set of fixed instrumental parameters the maximum crystal height for a crystal of over-all mosaic range γ_m is then

$$(h_c)_{\max} = (\alpha^v - (h_x/R_x) - 2\gamma_m \sin\theta)(R_x R_z/(R_x + R_z)) . \qquad \text{(D·3)}$$

For representative parameters, $\alpha^v = 2{\cdot}22°$, $h_x = 0{\cdot}1$ cm., $R_x = R_z = 14{\cdot}55$ cm., $\gamma_m = 0{\cdot}4°$, $\theta = 30°$:

$$(h_c)_{\max} = 0{\cdot}181 \text{ cm.}$$

It may be remarked, in conclusion, that any such calculated maximum value of the crystal height is valid only for perfect alignment in a vertical sense of the centers of the crystal, receiving collimator, and X-ray source. Any degree of misalignment will reduce the effective size of $(h_c)_{\max}$.

2. *Horizontal dimensions*

We shall first devote our attention to the 2θ-scan technique. From the mathematical development involved it will then be easy to deduce an expression for the ω-scan technique, which is geometrically the simpler of the two.

Referring to Fig. 31, we define the locations of the diffracted rays and receiving aperture in terms of $\Delta 2\theta$ units on the goniometer scale, the origin $2\theta_0$ being the calculated angle of diffraction for planes (hkl) and wavelength λ_0. Likewise the rotation of the crystal from its calculated angle of diffraction, ω_0, will be expressed in β units (refer to the beginning of section 5).

As illustrated in Fig. 31, when the crystal is turned through its entire angular range of reflection for X-rays of wavelength λ_0 from a source of width w_x, the diffracted rays move from a' to b'. In general, (1) rays a' and b' do not represent the minimum and maximum angles at which diffracted rays appear during this rotation of the crystal, and (2) the rays diffracted at any given instant comprise a bundle which occupies a finite angular range, $\Delta 2\theta$, in space.

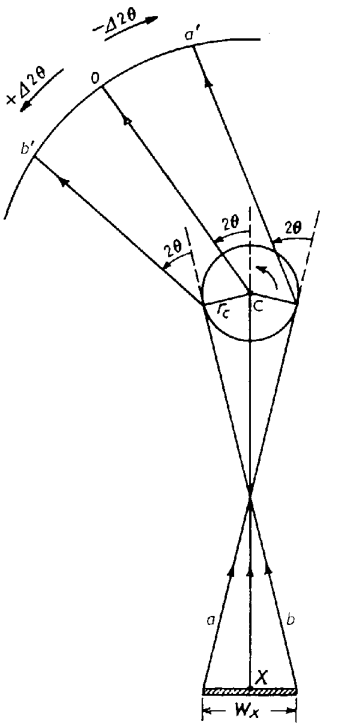

Fig. 31.

In the following treatment we shall define the angular locations of the leading and trailing edges of the receiving aperture, L and T, and of the diffracted ray bundle, L' and T', as functions of β. We again postulate that the receiver revolves through an angle 2β when the crystal turns through an angle β. We adopt the following nomenclature:

$\gamma_R = d_R/R_z$ = angular width of the receiver subtended at the crystal.
$\gamma_c = 2r_c/R_x$ = angular diameter of (cylindrical) crystal subtended at the X-ray source.
$\gamma_x = w_x/R_x$ = angular width of X-ray source subtended at the crystal.
γ_m = angular range of mosaicity of the crystal.
γ_λ = spectral dispersion on the θ scale.

When a cylindrical crystal of high transparency to X-rays is turned through its entire angular range of diffraction from planes (hkl), the cumulative diffraction effects are very nearly symmetrical about

$\Delta 2\theta = 0°$. During the diffraction process the crystal turns through the angular range $\pm \frac{1}{2}(\gamma_x + \gamma_m + \gamma_c + \gamma_\lambda)$ and the receiver through the range

$$\pm (\gamma_x + \gamma_m + \gamma_c + \gamma_\lambda) .$$

We first shall derive an expression for L' as a function of β. We initially consider a perfect crystal of radius r_c irradiated by a point source. We also postulate that $R_x \neq R_z$ and that r_c is very small with

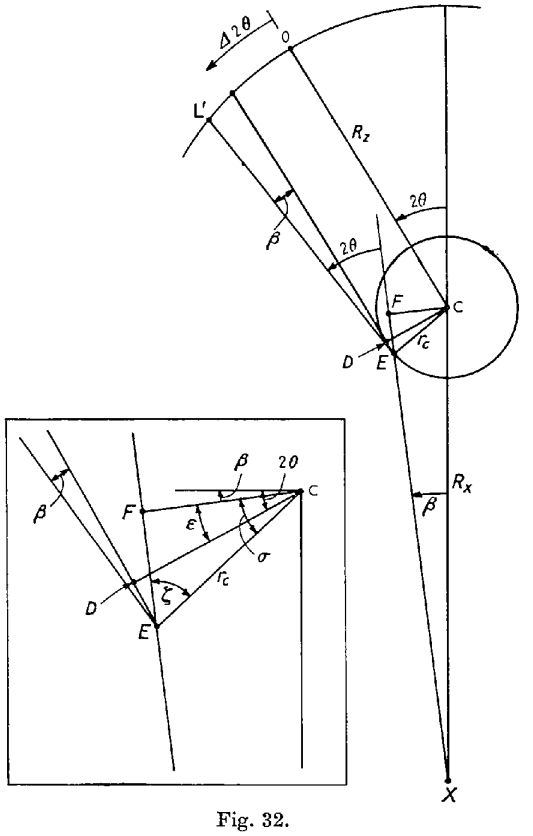

Fig. 32.

respect to R_x and R_z. Referring to Fig. 32, we see that

$$L' = CD/R_z + \beta .$$

By geometric and trigonometric equivalences

$$\begin{aligned} CD &= r_c \cos(\sigma - \varepsilon) \\ &= r_c \cos(\tfrac{1}{2}\pi - \zeta - 2\theta + \beta) \\ &= r_c \sin(\zeta + 2\theta - \beta) \\ &= r_c \{\sin\zeta \cos(2\theta - \beta) + \cos\zeta \sin(2\theta - \beta)\} \end{aligned}$$

But $\sin\zeta = R_x\beta/r_c$ and $\cos\zeta = [1 - (R_x\beta/r_c)^2]^{\frac{1}{2}}$, so that

$$CD = R_x\beta \cos(2\theta - \beta) + (r_c^2 - R_x^2\beta^2)^{\frac{1}{2}} \sin(2\theta - \beta) .$$

Making standard trigonometric substitutions for $\cos(2\theta - \beta)$ and $\sin(2\theta - \beta)$, and replacing $\sin\beta$ by β and $\cos\beta$ by 1, we find for CD:

$$\begin{aligned} CD = R_x\beta &[\cos 2\theta + \beta \sin 2\theta] \\ &+ (r_c^2 - R_x^2\beta^2)^{\frac{1}{2}} [\sin 2\theta - \beta \cos 2\theta] . \end{aligned}$$

Finally we obtain

$$\begin{aligned} L' &= (CD/R_z) + \beta \\ &= \tfrac{1}{2}\gamma_c((2\beta/\gamma_c) + (R_x/R_z)A) , \end{aligned}$$

wherein

$$\begin{aligned} A = 2\beta/\gamma_c &[\cos 2\theta + \beta \sin 2\theta] \\ &+ [1 - (2\beta/\gamma_c)^2]^{\frac{1}{2}} [\sin 2\theta - \beta \cos 2\theta] . \end{aligned} \quad \text{(D·4)}$$

Continuing to assign to β its particular significance in the above development, let us now also make allowance for the X-ray source width, mosaic spread of the crystal, and spectral dispersion. When the crystal has turned through the angle $\frac{1}{2}\gamma_x - \frac{1}{2}\gamma_m + \frac{1}{2}\gamma_\lambda + \beta$, the leading edge of the diffracted beam will have just reached the position

$$L' = \tfrac{1}{2}\gamma_x + \gamma_\lambda + \tfrac{1}{2}\gamma_c((2\beta/\gamma_c) + (R_x/R_z)A) , \quad \text{(D·5)}$$

and the leading edge of the receiving aperture will be at

$$L = \gamma_x - \gamma_m + \gamma_\lambda + 2\beta + \tfrac{1}{2}\gamma_R .$$

If we now let $\frac{1}{2}\gamma_x - \frac{1}{2}\gamma_m + \frac{1}{2}\gamma_\lambda + \beta_0$ be the crystal angle and A_0 the value of A corresponding to the minimal separation of the leading edges of the receiving aperture and diffracted beam, we may write:

$$(L - L')_{\min} = \tfrac{1}{2}\gamma_R + \tfrac{1}{2}\gamma_x - \gamma_m + \beta_0 - \tfrac{1}{2}\gamma_c(R_x/R_z)A_0 . \quad \text{(D·6)}$$

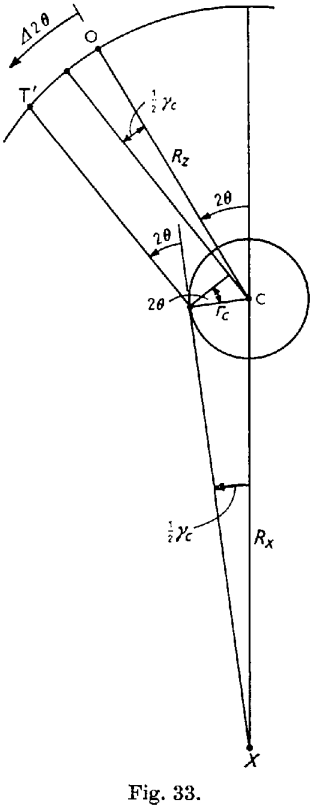

Fig. 33.

Equation (D·6) represents the greatest constraint upon the experimental parameters γ_R, γ_x, γ_m, γ_c, and R_x/R_z only when $R_x \gg R_z$ and over a very limited range of values of γ_c and 2θ. Acceptable values of the parameters correspond to $L-L' \geq 0$, from which the proper receiving aperture width is

$$\gamma_R \geq 2\gamma_m - \gamma_x - 2\beta_0 + \gamma_c(R_x/R_z)A_0 \,. \qquad \text{(D·7)}$$

Substitution of numerical quantities in (D·7) shows that when $R_x/R_z=1$ the maximum value of $(\gamma_R)_{\min}$ obtains when $\beta_0=0$, while for $R_x/R_z>1$, β_0 assumes values between 0 and $\frac{1}{2}\gamma_c$.

For the usual range of experimental conditions the greatest constraint upon the several experimental parameters is imposed by the minimum separation of the trailing edges of the diffracted rays and receiving aperture, $T'-T$. This situation occurs when the crystal has turned through its full range of diffraction and the diffracted ray bundle has dwindled to rays at the discrete angle

$$T'=L'=\tfrac{1}{2}\gamma_c[1+(R_x/R_z)\cos 2\theta] \,,$$

as shown in Fig. 33 for the simplified case of a perfect crystal of radius r_c irradiated by a point source. If we now add terms to allow for γ_x, γ_m, and γ_λ as in the prior derivation, the angle of the diffracted ray is

$$T'=L'=\tfrac{1}{2}\gamma_x+\gamma\ +\tfrac{1}{2}\gamma_c[1+(R_x/R_z)\cos 2\theta] \quad \text{(D·8)}$$

when the trailing edge of the receiving aperture is at

$$T=\gamma_x+\gamma_m+\gamma_\lambda+\gamma_c-\tfrac{1}{2}\gamma_R \,,$$

from which

$$T'-T=\tfrac{1}{2}\gamma_R-\tfrac{1}{2}\gamma_x-\gamma_m-\tfrac{1}{2}\gamma_c[1-(R_x/R_z)\cos 2\theta] \,.$$

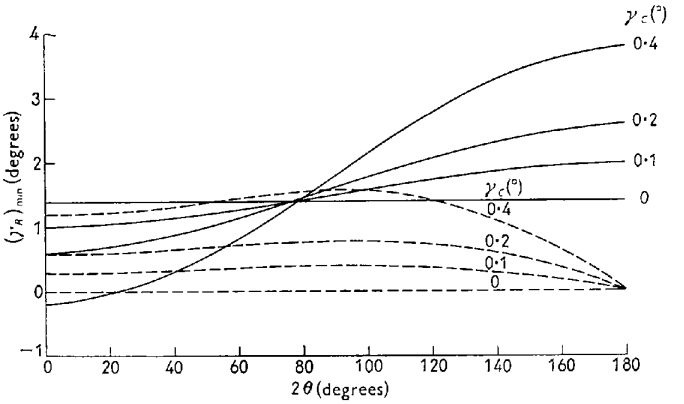

Fig. 35. Minimum receiving aperture width, $(\gamma_R)_{\min}$, as a function of 2θ for $R_x/R_z=4$, $\gamma_x=0{\cdot}70°$, $\gamma_m=0{\cdot}35°$, and four values of γ_c. Shown are results calculated with equation (D·7) (broken line) and equation (D·9) (solid line).

Hence, acceptable values of the parameters now correspond to $T'-T \geq 0$, or

$$\gamma_R \geq 2\gamma_m+\gamma_x+\gamma_c[1-(R_x/R_z)\cos 2\theta] \,. \qquad \text{(D·9)}$$

Fig. 34 depicts $(\gamma_R)_{\min}$ as a function of 2θ for several values of γ_c and γ_m and for the representative instrumental constants $\gamma_x=0{\cdot}70$ and $R_x/R_z=1$. These curves have been computed with the aid of equation (D·9) alone inasmuch as (D·7) takes precedence only within a limited range of experimental conditions when $R_x \gg R_z$, as mentioned earlier. The applicability of (D·7) in the low-2θ region is illustrated in Fig. 35 where it is seen to give the larger values of $(\gamma_R)_{\min}$ when $R_x/R_z=4$ and $\gamma_c>0{\cdot}2°$. At intermediate and large 2θ's, however, (D·9) again specifies the larger

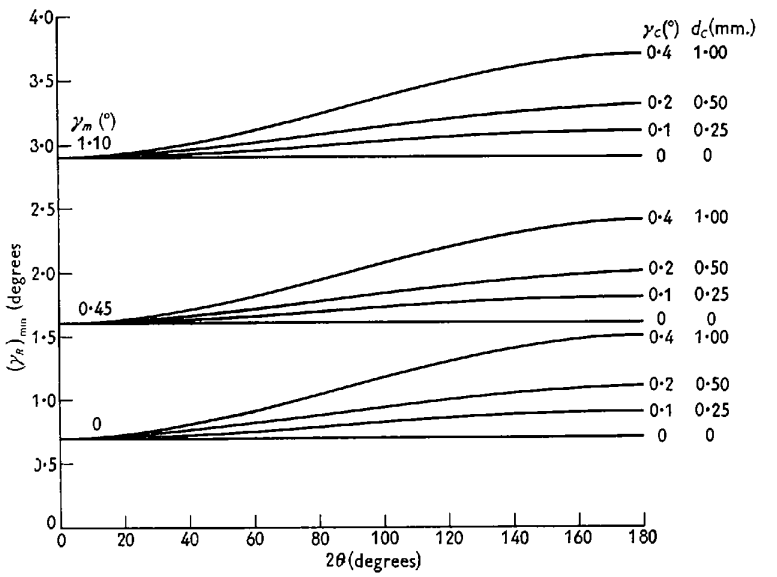

Fig. 34. Minimum receiving aperture width, $(\gamma_R)_{\min}$, as a function of 2θ for $R_x/R_z=1$ and $\gamma_x=0{\cdot}70°$ and for several values of γ_m and γ_c. The crystal diameter is given in degrees, γ_c (°), and also in mm., d_c (mm.), for the particular case $R_x=14{\cdot}55$ cm.

values and so takes precedence. It may be remarked that for most experimental work it is quite satisfactory to employ a goniometer for which $R_x/R_z=1$. As seen from Fig. 34, for this ratio there is little dependence of the minimum receiving aperture width upon crystal diameter at small Bragg angles.

We now are in a position to formulate an expression for the receiving aperture width pertinent to the ω-scan technique. Since the receiving aperture is stationary during the rotation of the crystal through its diffracting range, it is clear that its minimum width is simply equal to $2L'_{\max}$ as defined by equation (D·5):

$$\gamma_R \geq \gamma_x+2\gamma_\lambda+\gamma_c((2\beta/\gamma_c)+(R_x/R_z)A) . \quad \text{(D·10)}$$

It only remains to determine the maximum value of the last term in (D·10) for the appropriate range of experimental parameters. Substitution of numerical quantities shows that this term assumes a maximum value when $2\theta \rightarrow 0°$ and $2\beta \rightarrow \gamma_c$. Under these circumstances $A=1$ (refer to equation (D·4), and the expression of general applicability to the ω scan becomes

$$\gamma_R \geq \gamma_x+2\gamma_\lambda+\gamma_c[1+(R_x/R_z)] . \quad \text{(D·11)}$$

In this expression the numerical value to be assigned to $2\gamma_\lambda$ is in any case rather arbitrary inasmuch as its Cauchy-like profile exhibits no well defined angular limits. However, at large Bragg angles where $2\gamma_\lambda$ becomes of significant magnitude in relation to the other terms of (D·11), it is suggested that it be assigned a value at least equal to the angular separation of the $K\alpha$ doublet components plus five times the width at half-maximum intensity of either component, both on the 2θ scale. The absence in equation (D·9) of a term in γ_λ and in equation (D·11) of a term in λ_m shows that for minimum receiving aperture widths, other factors being equal, it is advantageous to employ the 2θ scan at large Bragg angles and the ω scan for highly mosaic crystals.

In conclusion a word of warning must be sounded regarding the significance of the quantities γ_c, α^v, and γ_R in the equations of this appendix. For a non-cylindrical crystal γ_c should be defined as the angular equivalent of the longest diagonal of its cross-section. The dimensions defined by equations (D·1), (D·7), (D·9), and (D·11) apply directly to *rectangular* apertures. For practical reasons, however, it may happen that the aperture is made circular, which places an additional restriction upon the dimensions of the diffracted beam. The upper limit that this factor can assume is given by the ratio of the edge of a square to the diameter of the smallest circle which can be circumscribed about it, which is $1/\sqrt{2}$. For this reason and also in recognition of the need for some tolerance between the dimensions of the beam and receiving aperture, it is suggested that in the calculation of minimal apertures, maximum crystal dimensions, etc., with the equations of this appendix, α^v and γ_R be replaced respectively by $\alpha^v/\sqrt{2}$ and $\gamma_R/\sqrt{2}$.

The authors are appreciative of Dr H. P. Klug's sustained interest in this investigation. They are grateful to Mr G. G. Sumner for writing the program for computing convolutions with the I.B.M. 650 Computer. They also wish to acknowledge the assistance of Mr D. F. Hales and Miss P. E. Brown with some of the experimental measurements and calculations.

References

ALEXANDER, L. E. (1950). *J. Appl. Phys.* **21**, 126.
ARNDT, U. W. (1960). *Acta Cryst.* **13**, 985.
ARNDT, U. W. & PHILLIPS, D. C. (1958). *Acta Cryst.* **11**, 509.
ARNDT, U. W. & PHILLIPS, D. C. (1961). *Acta Cryst.* **14**, 807.
BENEDICT, T. S. (1955). *Acta Cryst.* **8**, 747.
BOND, W. L. (1955). *Acta Cryst.* **8**, 741.
BROWN, P. J. & FORSYTH, J. B. (1960). *Acta Cryst.* **13**, 985.
BUERGER, M. J. (1942). *X-Ray Crystallography*, p. 301. New York: Wiley.
CLASTRE, J. (1960). *Acta Cryst.* **13**, 986.
CLIFTON, D. F., FILLER, A. & MCLACHLAN, D. (1951). *Rev. Sci. Instrum.* **22**, 1024.
COCHRAN, W. (1950). *Acta Cryst.* **3**, 268.
COMPTON, A. H. & ALLISON, S. K. (1935). *X-Rays in Theory and Experiment*. New York: Van Nostrand.
DRENCK, K., DIAMANT, H. & PEPINSKY, R. (1959). *American Crystallographic Association, Program and Abstracts*, Cornell University, Ithaca, New York, Abstract G-8.
EKSTEIN, H. & SIEGEL, S. (1949). *Acta Cryst.* **2**, 99.
EVANS, H. T. (1953). *Rev. Sci. Instrum.* **24**, 156.
FURNAS, T. C. (1957). *Single Crystal Orienter Instruction Manual*. Milwaukee: General Electric Company.
FURNAS, T. C. & HARKER, D. (1955). *Rev. Sci. Instrum.* **26**, 449.
LADELL, J. & LOWITZSCH, K. (1960). *Acta Cryst.* **13**, 205.
LADELL, J., PARRISH, W. & TAYLOR, J. (1959). *Acta Cryst.* **12**, 561, footnote p. 563.
LADELL, J., SPIELBERG, N. & LOWITZSCH, K. (1960). *Acta Cryst.* **13**, 986.
LANG, A. R. (1954). *Rev. Sci. Instrum.* **25**, 1039.
LONSDALE, K. (1948). *Acta Cryst.* **1**, 12.
WOOSTER, W. A., RAMACHANDRAN, G. N. & LANG, A. R. (1948). *J. Sci. Instrum.* **25**, 405.